Scribble1/AP2 Complex Coordinates NMDA Receptor Endocytic Recycling

Nicolas H Piguel, Sabine Fievre, Jean-Michel Blanc, Mario Carta, Maïté M Moreau, Enora Moutin, Vera L Pinheiro, Chantal Medina, Jerome Ezan, Léa Lasvaux, et al.

Article

Cell Reports

Scribble1/AP2 Complex Coordinates NMDA Receptor Endocytic Recycling

Graphical Abstract

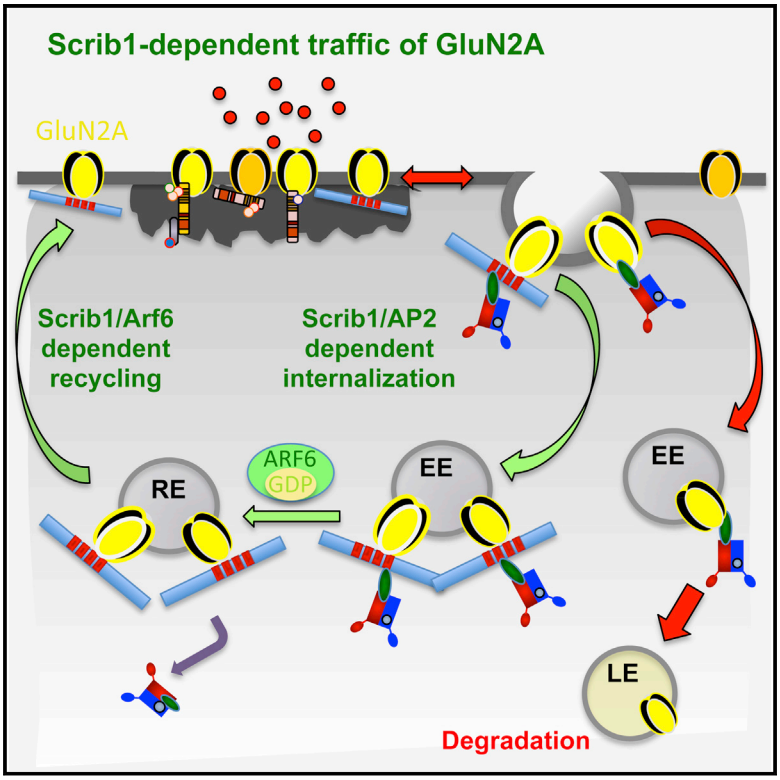

Authors

Nicolas H. Piguel, Sabine Fievre, ..., Claudia Racca, Nathalie Sans

Correspondence

nathalie.sans@inserm.fr

In Brief

Scribble1 (Scrib1) plays a major role in apico-basal and planar cell polarity in epithelial cells and was recently implicated in synaptic transmission and plasticity. Here, Piguel et al. report that Scrib1 is a key mediator of the endocytic sorting of NMDARs through its selective interactions with the AP2 complex. This Scrib1-dependent mechanism is likely to be involved in the regulation of synapse function in numerous physiological processes and pathological states that involve NMDARs.

Highlights

Scrib1 is regulated in an activity-dependent manner

Scrib1 drives the recycling of GluN2A subunits

AP2 interacts with Scrib1 YxxR motif to control NMDAR postendocytic traffic

Scrib1 is required for NMDAR maintenance at CA3-CA1 synapses

Piguel et al., 2014, Cell Reports 9, 712–727
October 23, 2014 ©2014 The Authors
http://dx.doi.org/10.1016/j.celrep.2014.09.017

OPEN ACCESS
CellPress

Cell Reports
Article

Scribble1/AP2 Complex Coordinates NMDA Receptor Endocytic Recycling

Nicolas H. Piguel,[1,2] Sabine Fievre,[3,4] Jean-Michel Blanc,[1,5,6] Mario Carta,[3,4] Maïté M. Moreau,[1,2] Enora Moutin,[7,8,9] Vera L. Pinheiro,[1,2] Chantal Medina,[1,2] Jerome Ezan,[1,2] Léa Lasvaux,[1,2] François Loll,[1,2] Christelle M. Durand,[1,2] Kai Chang,[10] Ronald S. Petralia,[10,11] Robert J. Wenthold,[10,14] F. Anne Stephenson,[12] Laurent Vuillard,[6] Hervé Darbon,[5] Julie Perroy,[7,8,9] Christophe Mulle,[3,4] Mireille Montcouquiol,[1,2] Claudia Racca,[13] and Nathalie Sans[1,2,*]

[1]Physiopathologie de la Plasticité Neuronale, Neurocentre Magendie, INSERM, U862, 33000 Bordeaux, France
[2]Neurocentre Magendie, University of Bordeaux, U862, 33000 Bordeaux, France
[3]Institut Interdisciplinaire de Neurosciences, University of Bordeaux, UMR 5297, 33000 Bordeaux, France
[4]Institut Interdisciplinaire de Neurosciences, CNRS, UMR 5297, 33000 Bordeaux, France
[5]Architecture et Fonction des Macromolecules Biologiques, UMR 7257, Campus de Luminy, CNRS/Aix-Marseille Universite, 13288 Marseille, France
[6]BioXtal Structural Biology Unit, Campus de Luminy, 13288 Marseille, France
[7]UMR-5203, Institut de Génomique Fonctionnelle, CNRS, 34000 Montpellier, France
[8]INSERM, U661, 34000 Montpellier, France
[9]Universités de Montpellier 1 and 2, UMR 5203, 34000 Montpellier, France
[10]Laboratory of Neurochemistry, National Institute on Deafness and Other Communication Disorders, National Institutes of Health, Bethesda, MD 20892, USA
[11]Advanced Imaging Core of NIDCD, National Institutes of Health, Bethesda, MD 20892, USA
[12]University College London School of Pharmacy, London WC1N 1AX, UK
[13]Institute of Neuroscience, Newcastle University, Newcastle upon Tyne NE2 4HH, UK
[14]Deceased
*Correspondence: nathalie.sans@inserm.fr
http://dx.doi.org/10.1016/j.celrep.2014.09.017

SUMMARY

The appropriate trafficking of glutamate receptors to synapses is crucial for basic synaptic function and synaptic plasticity. It is now accepted that NMDA receptors (NMDARs) internalize and are recycled at the plasma membrane but also exchange between synaptic and extrasynaptic pools; these NMDAR properties are also key to governing synaptic plasticity. Scribble1 is a large PDZ protein required for synaptogenesis and synaptic plasticity. Herein, we show that the level of Scribble1 is regulated in an activity-dependent manner and that Scribble1 controls the number of NMDARs at the plasma membrane. Notably, Scribble1 prevents GluN2A subunits from undergoing lysosomal trafficking and degradation by increasing their recycling to the plasma membrane following NMDAR activation. Finally, we show that a specific YxxR motif on Scribble1 controls these mechanisms through a direct interaction with AP2. Altogether, our findings define a molecular mechanism to control the levels of synaptic NMDARs via Scribble1 complex signaling.

INTRODUCTION

NMDA receptors (NMDARs) are widely distributed in the brain, where they play a key role in synapse development, synaptic transmission, and plasticity (Traynelis et al., 2010). GluN2A and GluN2B are differentially localized in neurons, and GluN2A is reportedly more stable and synaptic than GluN2B, which is more mobile and preferentially, but not exclusively, found at extrasynaptic sites (Lau and Zukin, 2007; Wenthold et al., 2003; Yashiro and Philpot, 2008). The polarized trafficking process of GluN2A and GluN2B has been intensively studied, but the pathways controlling NMDAR trafficking processes remain poorly understood (Lau and Zukin, 2007; Wenthold et al., 2003; Yashiro and Philpot, 2008).

*P*SD-95/*d*iscs-large/*Z*O-1 (PDZ) domain-containing proteins were identified as the major synaptic scaffolding proteins anchoring the NMDAR at glutamatergic synapses (Elias and Nicoll, 2007; Sheng and Hoogenraad, 2007). The initial PDZ-based interaction studies with membrane-associated guanylate kinases (MAGUKs) led to the identification of many PDZ proteins and their roles in glutamate receptor (GluR) anchoring and trafficking. It is now believed that NMDARs are dynamically associated with PDZ proteins that play various and specific roles in their trafficking to and/or from synapses, either by direct sorting, exocytosis from internal compartments, internalization, recycling, or lateral movements (Elias and Nicoll, 2007; Groc et al., 2009; Lau and Zukin, 2007; Sheng and Hoogenraad, 2007; Wenthold et al., 2003; Yashiro and Philpot, 2008). Synaptic NMDARs appear to be exchanged with extrasynaptic receptors and to be recycled through clathrin-dependent endocytosis, but NMDAR subunits seem to behave differently (Groc et al., 2006; Lavezzari et al., 2004; Montgomery et al., 2005; Pérez-Otaño et al., 2006; Prybylowski et al., 2005; Scott et al., 2004). GluN2A subunits are preferentially trafficked through the late endosome

pathway for degradation after internalization; GluN2B subunits are constitutively recycled (Lau and Zukin, 2007; Lavezzari et al., 2004). Moreover, during activation, the presence of GluN2A at synapses is favored and GluN2B is degraded (Barria and Malinow, 2002; Jurd et al., 2008). Several proteins, such as PDZ proteins (i.e., MAGUKs; Chung et al., 2004; Howard et al., 2010; Losi et al., 2003; Mauceri et al., 2007; Sans et al., 2003), soluble NSF attachment protein receptor (SNARE)-related proteins (Lau et al., 2010; Sans et al., 2003; Suh et al., 2010), or kinases (Prybylowski et al., 2005; Sanz-Clemente et al., 2010, 2013) can specifically affect membrane NMDAR subunit levels and the GluN2A/GluN2B ratio. This complex trafficking of NMDARs participates in the fine-tuning of excitatory synapses and in some types of long-term potentiation and long-term depression (Yashiro and Philpot, 2008).

Scribble1 (Scrib1) is a highly conserved protein that contains 16 leucine-rich repeat domains, two LAP domains, and four PDZ domains. Recently, we showed that Scrib1 participates in the development of hippocampal neurons and that a *circletail* mutant form impacts not only learning and memory but also social behavior (Moreau et al., 2010). Here, we decipher an original molecular and functional relationship between Scrib1 and NMDAR subunits that identifies Scrib1 as a key regulator of synaptic fine-tuning of excitatory synapses.

RESULTS

Scribble1 Interacts with the PDZ Binding Domain of the GluN2A and GluN2B Subunits

We performed a yeast two-hybrid screen with the PDZ domains of Scrib1 to probe a mouse P10 brain yeast two-hybrid library as described previously (Yi et al., 2007). We isolated a clone containing the sequence of GluN2A. In a two-hybrid screen with the C termini of the GluN2A subunit as bait, we isolated a clone that encoded the entire PDZ domain region of Scrib1. Consequently, we used the PDZ domains of Scrib1 as prey and found that pGBKT7-GluN2A or -GluN2B chimeras interacted strongly with these PDZ domains, whereas removal of the last seven amino acids of GluN2A or GluN2B (including the PDZ binding domain or PDZ-BD) prevented the interaction (Figure 1A). In human embryonic kidney 293 (HEK293) cells cotransfected with GFP-Scrib1, GFP-Scrib1ΔPDZ, and Tac-GluN2A or Tac-GluN2B chimeric transmembrane proteins, we were able to coimmunoprecipitate GFP-Scrib1. This interaction was lost upon deletion of the PDZ domains of Scrib1 (GFP-Scrib1ΔPDZ), indicating that Scrib1 interacts with NMDARs through its PDZ domain (Figure 1B). In pull-down experiments, the PDZ domains 2 and 3 of Scrib1 were able to bind independently to GluN2A and GluN2B fusion proteins (data not shown). Isothermal titration calorimetry (ITC) experiments revealed that both the GluN2A and GluN2B peptides bound to PDZ2 with a K_D of approximately 60 μM for GluN2A and 48 μM for GluN2B and to PDZ3 with a K_D of 11.6 μM for GluN2A and 12.3 μM for GluN2B. The binding of PDZ4 was weaker, with a K_D over 150 μM, whereas no binding was observed with PDZ1 (Figures 1C and 1D; Table S1). We also tested the PDZ binding domain mutant peptides (GluN2A^{S1462A} and GluN2B^{S1480A}) and observed no binding (Figures 1E and 1F; Table S1). Taken together, these data demonstrate that Scrib1 PDZ2 and PDZ3 interact specifically with the PDZ-BD of the GluN2A and GluN2B subunits.

The Spatio temporal Localization of Scribble1 Matches that of NMDARs

We examined the temporal expression and localization of Scrib1 in the rat brain. As illustrated in Figure 1G, Scrib1 expression level decreased from postnatal day 0 (P0) to adult with a persistent expression at P120. Other related proteins, such as densin-180 and Erbin, displayed different developmental profiles (Figure 1G). The early and strong expression of Scrib1 matches that of GluN2B and overlaps with GluN2A in later stages (starting at P9), which is consistent with an interaction of Scrib1 with the GluN subunits. The interaction of Scrib1 with the GluN1, GluN2A, and GluN2B subunits, but not with the $GABA_A$ receptor β3 subunit, was confirmed by coimmunoprecipitation (coIP) (Figure 1H).

Using postembedding immunogold electron microscopy, we showed that Scrib1 is localized with NMDARs postsynaptically at excitatory synapses in the stratum radiatum of the CA1 region of the hippocampus (Figures 1I–1K and S1A–S1G; Scrib1: 5 nm gold particles and GluN1: 15 nm gold particles). We also found Scrib1 associated with NMDARs in intracellular vesicles or organelles in the dendritic spine (Figures S1H and S1I). These localizations are consistent with our in vitro data and coIP experiments.

Scrib1 and GluN2A Levels Increase at Active Synapses

To investigate whether the levels of Scrib1 were relevant for function, we analyzed whether they were regulated by synaptic activity. We used the Na^+ channel blocker tetrodotoxin to block synaptic activity or the $GABA_A$ receptor antagonist bicuculline to increase excitatory activity by blocking inhibitory GABAergic transmission in cultured neurons. Enriched synaptosome preparations showed that Scrib1 levels mirrored GluN2A profile of expression and accumulated in active synaptosome fractions (Figures 2A and 2B). These data suggest that levels of Scrib1 and GluN2A-containing NMDARs are correlated and that Scrib1 participates in NMDAR regulation at the membrane to modify synaptic strength.

To investigate whether Scrib1 and NMDAR levels were also regulated by activity in vivo, we examined whether exposure of adult rats to a new enriched environment modified Scrib1 and NMDAR levels. Rats were subjected to an enriched open field for 10 min and left undisturbed in their home cages for 1 hr before collecting the hippocampus (enriched open field [EOF] animals), whereas control group rats were placed in their home cages until tissue collection (control; Figure 2C). Results showed that Scrib1 levels increased significantly in hippocampi of EOF rats compared to the control group ($p < 0.01$; Figure 2D). This upregulation of Scrib1 in the hippocampus of EOF rats was accompanied by a significant increase of GluN2A and a slight but significant reduction of GluN2B in the synaptosomal fraction ($p < 0.05$; Figure 2E). In hippocampal membrane fraction, Scrib1 coimmunoprecipitated GluN2A around 30% more in EOF condition than in basal conditions whereas the levels of GluN2B were not significantly different (Figures 2F and 2G). These results show that exposure to a new environment leads to a major increase in

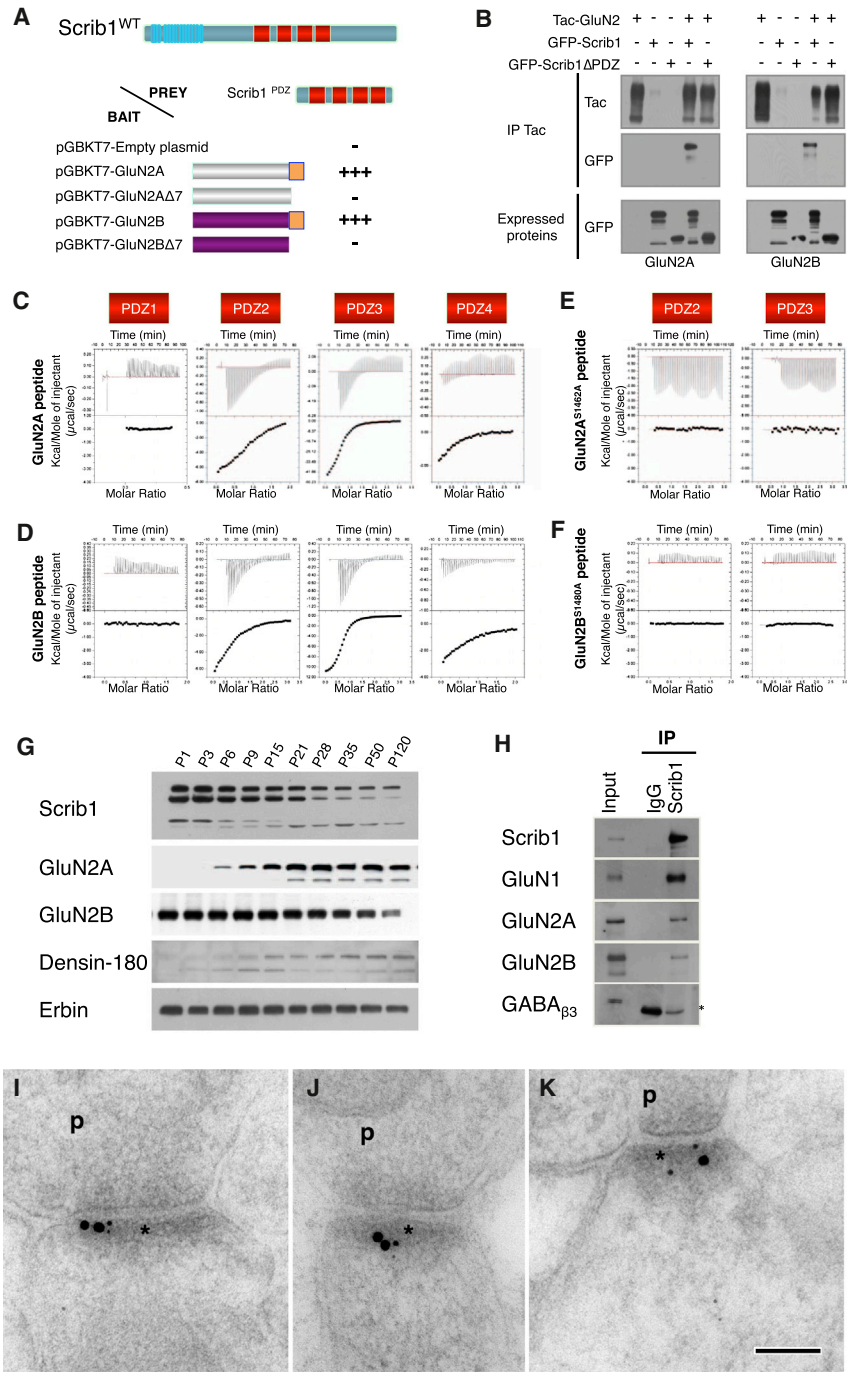

Figure 1. Scrib1 Interacts and Colocalizes with GluN2 Subunits

(A) Directed yeast two-hybrid assays with GluN2A, GluN2B, and Scrib1 constructs. Schematic domain structures of GluN2 C-terminal used as bait. Scrib1 binds the PDZ binding domain of GluN2A and GluN2B. For the same concentration and same dilution, >40 colonies grew on 4DO plates for 2A and 2B baits whereas none for Δ7 constructs after 4 days at 30°C.

(B) Lysates from HEK293 cells transfected with GFP-Scrib1 or GFP-Scrib1$^{\Delta PDZ}$ and Tac-GluN2A or Tac-GluN2B and immunoprecipitated with Tac antibodies. The precipitates were immunoblotted with anti-GFP or anti-Tac. GFP-Scrib1 coimmunoprecipitates with Tac-GluN2A and TacGluN2B.

(C–F) Calorimetric titrations of Scrib1 PDZs interaction with GluN2A (C), GluN2B (D), GluN2A^{S1462A} (E), and GluN2B^{S1480A} (F) peptides. Top: ITC heat variation after each ligand; the first peak corresponds to a small amount of injected ligand. Bottom: the corrected heat developed per mole of ligand. This curve allows the determination of the dissociation constant using the theory of Wiseman isotherm.

(G) Developmental protein expression pattern of Scrib1 and the GluN2A and GluN2B from P1 to P120 in rat hippocampus homogenates (30 μg protein per lane) analyzed by SDS-PAGE and immunoblotted with the antibodies described in the Supplemental Experimental Procedures. At all ages, the samples were analyzed with the different antibodies obtained from the same preparation of hippocampus. Representative results, n = 3 experiments.

(H) Endogenous coIP of Scrib1, GluN2A, and GluN2B from the hippocampus. The 100,000 × g detergent supernatants were immunoprecipitated with Scrib1 antibodies. The precipitates show positive immunoblotting for GluN2A and GluN2B subunits, but not β3-containing $GABA_A$ receptor (star, bands in IP correspond to immunoglobulin G [IgG]).

(I–K) Immunogold localization of Scrib1 (5 nm) and its colocalization with GluN1 (15 nm) in hippocampal CA1 stratum radiatum synapses. Note the double labeling in PSD. Asterisk, postsynaptic density; p, presynaptic terminal. The scale bar represents 100 nm.

Scrib1 expression and modifies the amount of Scrib1-NMDAR subunit content in the hippocampus.

Scrib1 Levels Regulate Native NMDA Surface Receptors in Hippocampal Neurons

To determine the consequences of the levels of Scrib1 on the surface expression of native GluN2A and GluN2B receptors, we used loss- and gain-of-function approaches. We used the N-terminal antibodies developed against GluN2A (Groc et al., 2006) and the commercially available N-terminal GluN2B from Alomone Labs. Number of puncta and global intensity of native GluN2A or GluN2B increased in the presence of GFP-Scrib1 protein (GluN2A puncta: Ctrl: 23.33 ± 0.75 versus Scrib1: 27.75 ± 0.99, $p < 0.05$; intensity: 74.67 ± 2.55 versus 90.23 ± 3.96, $p < 0.01$; GluN2B puncta: 20.97 ± 0.64 versus 25.22 ± 1.26, $p < 0.01$; intensity: 96.57 ± 3.85 versus 113.73 ± 5.25, $p < 0.05$; Figures 3A, 3B, 3D, and 3E), whereas surface staining for both subunits was not different in the presence of a mutated form of Scrib1 missing the two PDZ domains implicated in the interaction with NMDAR (GluN2A puncta: Ctrl: 23.33 ± 0.75 versus GFP-Scrib1$^{\Delta PDZ2\text{-}3}$: 21.51 ± 0.61, $p = 0.065$; intensity: 74.67 ± 2.55 versus 78.47 ± 3.25, $p = 0.36$; GluN2B puncta: 20.97 ± 0.64 puncta versus

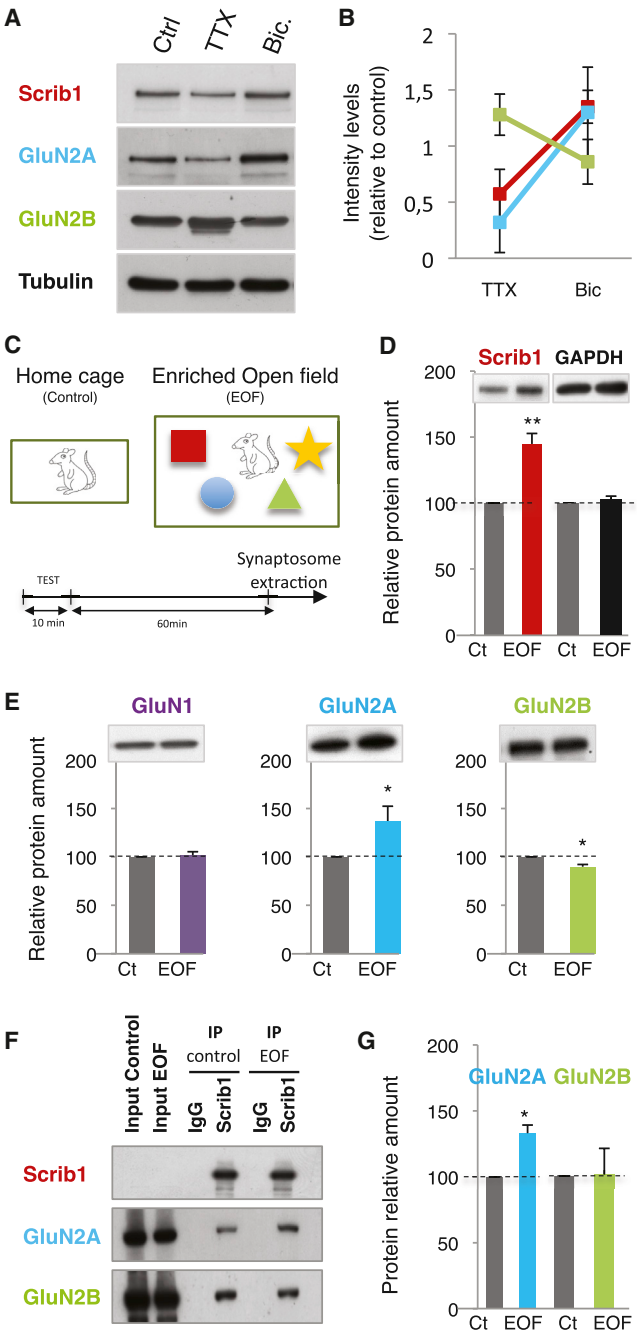

Figure 2. Expression of Scrib1 and GluN Proteins Is Regulated by Activity in the Hippocampus

(A) Immunoblot analysis of Scrib1, GluN2A, GluN2B, and tubulin in synaptic fractions isolated from cortical neurons treated 48 hr with control solution, TTX (2 μM), or bicuculline (Bic.) (40 μM).

(B) Quantitative analysis of the abundance of Scrib1 (red), GluN2A (blue), and GluN2B (green) in synaptic fractions treated with TTX or bicuculline of the band intensities 48 hr after drug treatment and normalized to the control values from the untreated control neuron synaptic fraction. Note that abscissa values reflect drug treatments. All data are presented as mean ± SEM (n = 3 experiments). Error bars are all ± SEM.

(C) Experimental design protocol of the hippocampal synaptosome extraction after new environment stimulation in an enriched open field (EOF).

(D) Quantitation of Scrib1 and GAPDH levels in hippocampus extracts by western blot.

(E) Western blot of GluN1, GluN2A, and GluN2B protein in P2 subcellular fractionation of rat hippocampus lysates. Error bars are all ± SEM.

(F) Endogenous coIP of GluN2A and GluN2B with Scrib1 from the hippocampus of control or EOF rats. The 100,000 × g detergent supernatants were immunoprecipitated with anti-Scrib1. Ten microliters of bound immunoprecipitate fractions were separated by SDS-PAGE; immunoblotted; and incubated with Scrib1, GluN2A, or GluN2B antibodies. Percentage of immunostaining in the bound fraction is shown in (G).

(G) Quantitation of the IP bands normalized to control (100% = control gray histograms). Levels were measured using the ChemiDoc MP imager system. There is a significant difference in GluN2A-bound fraction to Scrib1 in the EOF compared to control condition. Error bars are all ± SEM.

20.35 ± 0.52, p = 0.45; intensity: 96.57 ± 3.85 versus 97.2 ± 3.86, p = 0.48; Figures 3A, 3C, 3D, and 3F). On the other hand, downregulation of Scrib1 led to a decrease of the density of surface staining of native GluN2A or native GluN2B (GluN2A: small hairpin control [shCtrl]: 23.69 ± 0.67 versus shScrib1: 16.82 ± 0.83, $p < 0.001$; GluN2B: 20.03 ± 0.85 versus 16.23 ± 0.49, $p < 0.01$; Figures 3G, 3H, 3J, and 3K). The total intensity for GluN2A in dendrites measured as the ratio of the surface-staining intensity per unit area was also decreased (69.99 ± 2.81 versus 58.05 ± 2.9, $p < 0.05$; Figures 3G and 3I). Surprisingly, a similar quantification revealed no change in this ratio for GluN2B (92.96 ± 4.48 versus 104.02 ± 4.32, p = 0.08; Figures 3J and 3L). We found the same trend with transfected myc-GluN2A or myc-GluN2B (Figure S2). We were able to rescue the sh-induced phenotype using an sh-resistant form of Scrib1, but not with the mutated form of Scrib1 missing the two PDZ domains (GluN2A/shScrib1 puncta: rescue by Scrib1: 24.42 ± 0.78 versus no rescue by GFP-Scrib1$^{\Delta PDZ2-3}$: 16.11 ± 0.46, $p < 0.001$; intensity: 74.99 ± 3.66 versus 57.09 ± 3.32, $p < 0.01$; GluN2B/shScrib1 puncta: rescue: 21.89 ± 0.9 versus no rescue: 16.09 ± 0.53, $p < 0.01$; intensity: 94.62 ± 4.47 versus 104.64 ± 5.43, p = 0.17; Figures 3G–3I and 3J–3L). Scrib1 overexpression or downregulation had no impact on native α1-containing $GABA_A$ receptors (Figures 3M and 3N) or on the number of synapses (Figures 3O and 3P). Altogether, our results show that Scrib1 levels affect NMDA surface receptors via PDZ2 and PDZ3 interaction with GluN2 because the Scrib1 mutated form missing these two specific domains has no effect on NMDAR trafficking.

Differential Regulation of Native NMDA Surface Receptors after D-Serine Stimulation prior to NMDA/D-Serine Activation

To investigate whether a stimulation of the receptors could differently modify the surface expression of NMDAR depending on Scrib1 levels, we compared basal conditions to D-serine stimulation prior to NMDA/D-serine activation, thus "priming" the NMDAR (Nong et al., 2003). After stimulation, surface staining of native GluN2A increased with increased Scrib1 levels and decreased with decreased Scrib1 levels as shown previously without stimulation (GluN2A puncta: Ctrl: 24.97 ± 0.56 versus Scrib1: 29.28 ± 0.84 puncta, $p < 0.001$; shCtrl: 24.36 ± 0.34 versus shScrib1: 20.92 ± 0.38, $p < 0.001$; Figures S3A and S3B). Total intensity varied in the same manner (Figures S3A and S3B). However, after stimulation, surface staining of native GluN2B

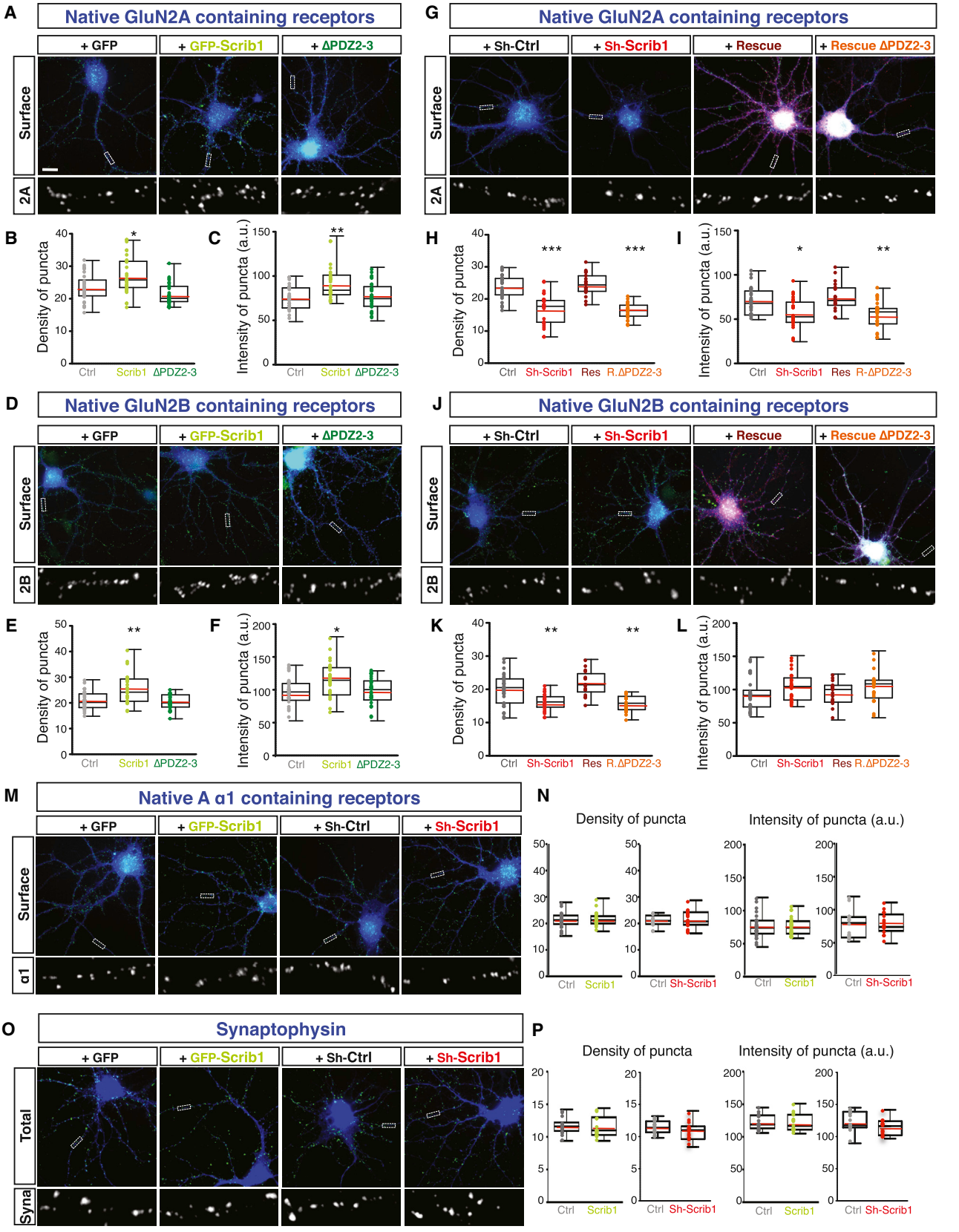

(legend on next page)

decreased with increased Scrib1 levels and increased with decreased Scrib1 levels (GluN2B puncta: Ctrl: 19.00 ± 0.52 versus Scrib1: 16.58 ± 0.64, $p < 0.01$; shCtrl: 19.05 ± 0.47 versus shScrib1: 22.69 ± 0.4, $p < 0.001$; Figures S3C and S3D). The total intensity varied in the same manner (Figures S3C and S3D). Altogether, these data suggest that Scrib1 regulates the pool of surface GluN2A and GluN2B dynamically, depending on neuronal activity context, and the stimulation or not of NMDARs affect differently the pool of surface GluN2A and GluN2B.

Scrib1 Interacts with Tac-GluN2A and Tac-GluN2B Chimeras at the Plasma Membrane and in Endosomes of COS-7 Cells

To investigate the involvement of Scrib1 in NMDAR internalization and recycling, we carried out experiments in COS-7 cells with NMDAR subunit chimeras. In these cells, Scrib1 was redistributed and colocalized with GluN2 chimeras at the plasma membrane and in vesicle-like clusters (Figures S4A and S4B) and the removal of the PDZ-BD of the chimeras (Tac-GluN2AΔ7 or Tac-GluN2BΔ7) abolished this redistribution (Figures S4C and S4D).

The localization of the GluN2 chimeras-Scrib1 complex in intracellular clusters suggests two nonmutually exclusive possibilities: (1) these clusters are involved in the sorting of GluN2 chimeras from the Golgi complex to the plasma membrane and/or (2) Scrib1 is associated with internalized receptors. First, surface staining was performed to validate that some of the Scrib1 puncta colocalized with surface Tac-GluN2A and Tac-GluN2B chimeras (data not shown). After 15 min of internalization, we observed a complete colocalization of Scrib1/internalized GluN2 chimeras with Rab5a (Figures S4E and S4F). After 30 min of internalization, the majority of Tac-GluN2A was colocalized with CD63 in late endosomes and lysosomes and only 20% was associated with Rab11 in recycling endosomes (Figures S4G and S4H) as previously published (Lavezzari et al., 2004). In the presence of Scrib1, we observed a shift in the localization of the GluN2A chimeras, with 40% of the GluN2A chimeras found in Rab11-positive recycling endosomes (Figures S4G, S4H, S4K, and S4L). Scrib1 expression slightly increased the colocalization of GluN2B with Rab11 in recycling endosomes (Figures S4I and S4J) and decreased the colocalization with CD63 (Figures S4M and S4N). Scrib1 promotes GluN2A chimera recycling (Figures S4O and S4P) and to a lesser extent GluN2B chimera recycling (Figures S4Q and S4R). These results show that Scrib1 participates in Tac-GluN2A and Tac-GluN2B internalization and favors the recycling pathway in COS-7.

Scrib1 Levels Differentially Modulate myc-GluN2A and myc-GluN2B Internalization in Hippocampal Neurons

Next, we wanted to determine whether Scrib1 affected specifically internalization or recycling of GluN2A and/or GluN2B subunits in hippocampal neurons. First, we examined whether an upregulation or downregulation of Scrib1 could modulate internalization of GluN2 subunits (Figure 4A). Because these experiments require a large amount of antibodies, we used surface-expressed receptors. We also compared basal conditions to D-serine stimulation after priming the NMDAR for endocytosis, as before. Increasing Scrib1 levels did not change the internalized/surface ratio of myc-GluN2A or myc-GluN2B (Ps > 0.1; Figures 4B, 4C, 4F, and 4H). The activation of NMDARs significantly reduced the surface expression of myc-GluN2A independently of Scrib1 levels (stimulus effect: $p < 0.001$; treatment effect: $p = 0.10$; Figures 4B and 4F). Decrease of Scrib1 levels had the opposite effect on the internalization of both subunits (Figures 4D, 4E, 4G, and 4I). In basal conditions, a decrease of Scrib1 levels increased the internalization/surface ratio of GluN2A, whereas this ratio was decreased for GluN2B ($p < 0.001$; Figures 4D, 4E, 4G, and 4I). The activation of NMDARs in neurons with decreased Scrib1 levels abolished the effect seen in basal conditions for GluN2B ($p > 0.3$; Figures 4D, 4E, 4G, and 4I). Using an sh-resistant form of Scrib1, we could rescue the sh-induced phenotype for GluN2A (Figures 4J and 4K) or GluN2B (Figures 4L and 4M) in basal conditions. Together, these data show that the upregulation of Scrib1 does not change the internalized/surface ratio of either GluN2A or GluN2B in basal or activated conditions. On the other hand, the downregulation of Scrib1 has a differential effect on the internalized/surface ratio of GluN2A and GluN2B.

Scrib1 Facilitates myc-GluN2A Recycling in Hippocampal Neurons

We tested whether Scrib1 levels modulated NMDAR subunit recycling after internalization in neurons (Figure 5A). Recycling experiments under basal conditions showed that increased Scrib1

Figure 3. Modification of Scrib1 Levels Affects Surface Expression of Endogenous GluN2A and GluN2B-Containing Receptors

(A–C) Surface staining of endogenous GluN2A-containing NMDAR with overexpression of GFP-control, GFP-Scrib1, or GFP-Scrib1ΔPDZ2-3 in primary hippocampal neuron culture (A) and box-and-whisker plots indicate the median value (black line) and mean value (red line), the 25th–75th (box), and the 10th–90th (whiskers); open circles represent individual values for GluN2A puncta number (B) or intensity (C).

(D–F) Surface staining of endogenous GluN2B-containing NMDAR with overexpression of GFP-control, GFP-Scrib1, or GFP-Scrib1ΔPDZ2-3 in primary hippocampal neuron culture (D) and box-and-whisker plots; open circles represent individual values for GluN2B puncta number (E) or intensity (F).

(G–I) Surface staining of endogenous GluN2A-containing NMDAR with overexpression of sh-control, sh-Scrib1, or rescue with Scrib1 or Scrib1ΔPDZ2-3 in primary hippocampal neuron culture (G) and box-and-whisker; open circles represent individual values for GluN2A puncta number (H) or intensity (I).

(J–L) Surface staining of endogenous GluN2B-containing NMDAR with overexpression of sh-control, sh-Scrib1, or rescue with Scrib1 or Scrib1ΔPDZ2-3 in primary hippocampal neuron culture (J) and box-and-whisker plots; open circles represent individual values for GluN2B puncta number (K) or intensity (L).

Data were compared using Kruskal-Wallis one way with Dunn's multiple comparison. a.u., arbitrary units (n = 20–30 neurons).

(M and N) Surface staining of endogenous α1-containing GABAAR with overexpression of GFP-control or GFP-Scrib1 and sh-control or sh-Scrib1 in primary hippocampal neuron culture (M) and box-and-whisker plots; open circles represent individual values puncta number (left) or intensity (right; N).

(O and P) Surface staining of endogenous synaptophysin with overexpression of GFP-control or GFP-Scrib1 and sh-control or sh-Scrib1 in primary hippocampal neuron culture (O) and box-and-whisker plots; open circles represent individual values puncta number (left) or intensity (right; P).

Data were compared using t test (n = 15–26 neurons). The scale bar represents 10 μm.

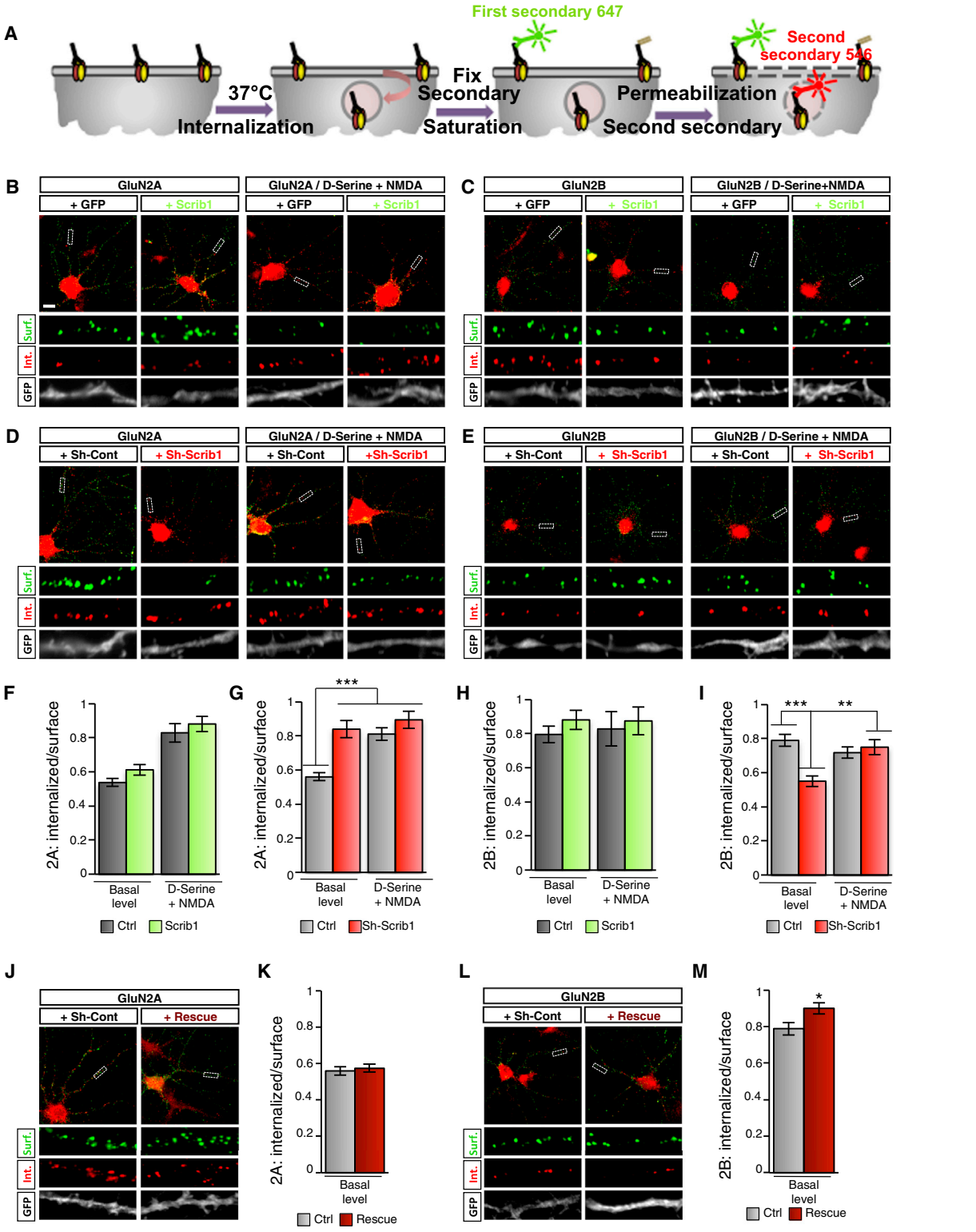

Figure 4. The Loss of Scrib1 Stabilizes GluN2B and Increases GluN2A Internalization

(A) Timeline of the endocytosis experiments.

(B and C) Internalization of GluN2A-containing NMDARs (B) and GluN2B-containing NMDARs (C) with or without stimulation, respectively. Primary hippocampal neuron cultures were transfected with myc-GluN2A (B) or myc-GluN2B (C) and GFP-control or GFP-Scrib1 at 14 or 15 DIV.

(legend continued on next page)

levels specifically increased the recycling of internalized myc-GluN2A back to the plasma membrane, which is otherwise degraded ($p < 0.001$; Figures 5B and 5F), but had no effect on GluN2B ($p = 0.79$; Figures 5C and 5H) or $GABA_A$ receptor β3 subunit ($p = 0.99$; data not shown). Additional activation of NMDARs further increased recycling of the internalized GluN2A back to the plasma membrane in the presence of overexpressed Scrib1 ($p < 0.01$; Figures 5B and 5F) and significantly decreased the recycling of GluN2B, independently of Scrib1 overexpression ($p < 0.001$; Figures 5C and 5H). Thus, NMDARs activation influenced differently the recycling traffic of GluN2A and GluN2B in the presence of Scrib1 through a specific GluN2A recycling increase whereas GluN2B recycling appeared insensitive to Scrib1 increased levels.

Loss-of-function experiments were done to evaluate the impact of decreased levels of Scrib1 expression. Under basal conditions, decreased Scrib1 levels did not affect the recycling rate of GluN2A at the membrane ($p = 0.70$; Figures 5D and 5G). NMDAR activation slightly increased the recycling of GluN2A, which was abolished in the absence of Scrib1 ($p < 0.05$; Figures 5D and 5G). Under basal conditions, downregulation of Scrib1 levels significantly decreased GluN2B recycling at the membrane ($p < 0.001$; Figures 5E and 5I). Notably, NMDAR activation changed the ratio of recycled/internalized GluN2B; here, downregulation of Scrib1 increased the recycling of GluN2B compared to control shRNA ($p < 0.001$). To further decipher the Scrib1-dependent trafficking pathway, we performed endosomal staining in neurons transfected with GFP-Rab11 and GFP-CD63, 30 min after internalization of myc-GluNs in the presence of hemagglutinin (HA)-Scrib1 (Figure S5) or mCherry-pSuper-Scrib1 (Figure S6). As expected, we observed a stronger colocalization of GluNs with Rab11 than with CD63 for all the conditions showing an increasing recycling. On the contrary, a decrease in recycling was always associated with a stronger colocalization with CD63 at the expense of Rab11 (Figures S5 and S6). In conclusion, GluN2A and GluN2B behave differently in response to the expression level of Scrib1: Scrib1 upregulation affects the recycling of GluN2A more than that of GluN2B, whereas Scrib1 downregulation blocks GluN2A recycling, with opposite effects on GluN2B recycling depending on the activation state of the neuron.

We wanted to study the role of ARF6 in the regulation of NMDAR by Scrib1, as it is a known regulator of other transmembrane receptor (Lahuna et al., 2005). Interestingly, ARF6 increased GluN2A recycling and $ARF6^{T27N}$ (a dominant-negative form) inhibited Scrib1-dependent effect on recycling (Figures 5J and 5K). Expression of a catalytically inactive form of ARF6 guanine nucleotide exchange factor EFA6 (EFA6-E242K), known to regulate constitutive endosomal recycling to the cell surface (Franco et al., 1999), also inhibited Scrib1-induced effect on recycling (Figures 5L and 5M). These results strongly suggest that Scrib1 regulates the recycling of GluN2A through ARF6 activation.

The AP2 Adaptor Interacts with Scrib1 to Allow Internalization and Recycling of the NMDAR/Scrib1 Complex

Several studies have shown that PDZ proteins, such as PSD-95, stabilize NMDARs at the membrane (Groc et al., 2006; Prybylowski et al., 2005; Roche et al., 2001). In the case of GluN2B-containing NMDARs, the PDZ protein dissociates from the receptor to allow the AP2 adaptors to bind a distal YEKL motif on the GluN2B tail and to induce its internalization, which is followed by a rapid recycling of the synaptic receptor (Prybylowski et al., 2005; Scott et al., 2004). The GluN2A subunit is regulated differently (Prybylowski et al., 2005). Because Scrib1 is a PDZ protein that colocalizes with GluRs at the membrane and in endocytic vesicles, it was difficult to reconcile our data with this model. We also noticed in our electron microscopic analysis that Scrib1 was sometime present at the lateral domain of the spine (Figure 6A), where activity-dependent exocytosis and endocytosis domains have been identified (Kennedy et al., 2010). In our yeast two-hybrid screen with the PDZ-containing domains of Scrib1, we found a clone containing an ~0.7 kb insert encoding amino acids 200–429 of the open reading frame of the AP2μ subunit (NP_033809.1). Sequence analysis showed that this clone contained the C-terminal domain of AP2μ, which recognizes tyrosine-based sorting motifs, such as YxxØ (where x is a polar or charged amino acid and Ø is a hydrophobic residue; Traub, 2009). We found one putative binding site for AP2 close to the consensus sequence found in vertebrates in the Scrib1 sequence between PDZ1 and PDZ2 (Figure 6B). This sequence (YSPR) differs from the consensus sequence for AP2 binding site in substitution of the Y+3 hydrophobic residue with a charged arginine. However, it should be noted that Arg was found in this position in other proteins that bind AP2 adaptors with a strong affinity (Uekita et al., 2001). The mutation of one amino acid in this sequence prevented Scrib1 binding to AP2 both in a yeast two-hybrid assay and pull-down experiments (Figures 6C and 6D). We further validated this interaction by coimmunoprecipitation of AP2 in hippocampal lysates from P21 rats using an antibody against Scrib1 (Figure 6E). We then modeled the binding of our target sequence to AP2μ. The

(D and E) Internalization of GluN2A-containing NMDARs (D) and GluN2B-containing NMDARs (E) with or without stimulation, respectively. Primary hippocampal neuron cultures were transfected with myc-GluN2A (D) or myc-GluN2B (E) and sh-control or sh-Scrib1 at 14 or 15 DIV.
Surface receptor populations are labeled in green, and internalized receptor populations are in red.
(F–I) Histograms represent the means of the ratio of internalized puncta over the surface receptor puncta, corresponding, respectively, to the images in (B)–(E). (F) Data were compared using two-way ANOVA (n = 19 to 20 neurons). (G) Data were compared using two-way ANOVA and Bonferroni multiple comparison test (n = 15–20 neurons). (H) Data were compared using two-way ANOVA (n = 16–20 neurons). (I) Data were compared using two-way ANOVA and Bonferroni multiple comparison test (n = 15–17 neurons) ± SEM. Error bars are all ± SEM.
(J and K) Internalization of GluN2A-containing NMDARs with sh-control or sh-Scrib1 and shRNA-resistant HA-Scrib1 form (rescue; J) and histograms represent the means of the ratio of internalized puncta over the surface receptor puncta (K). Error bars are all ± SEM.
(L and M) Internalization of GluN2B-containing NMDARs with sh-control or sh-Scrib1 and shRNA-resistant HA-Scrib1 form (rescue; L) and histograms represent the means of the ratio of internalized puncta over the surface receptor puncta (M). Error bars are all ± SEM.
Data were compared using an unpaired t test ± SEM. The scale bar represents 10 μm.

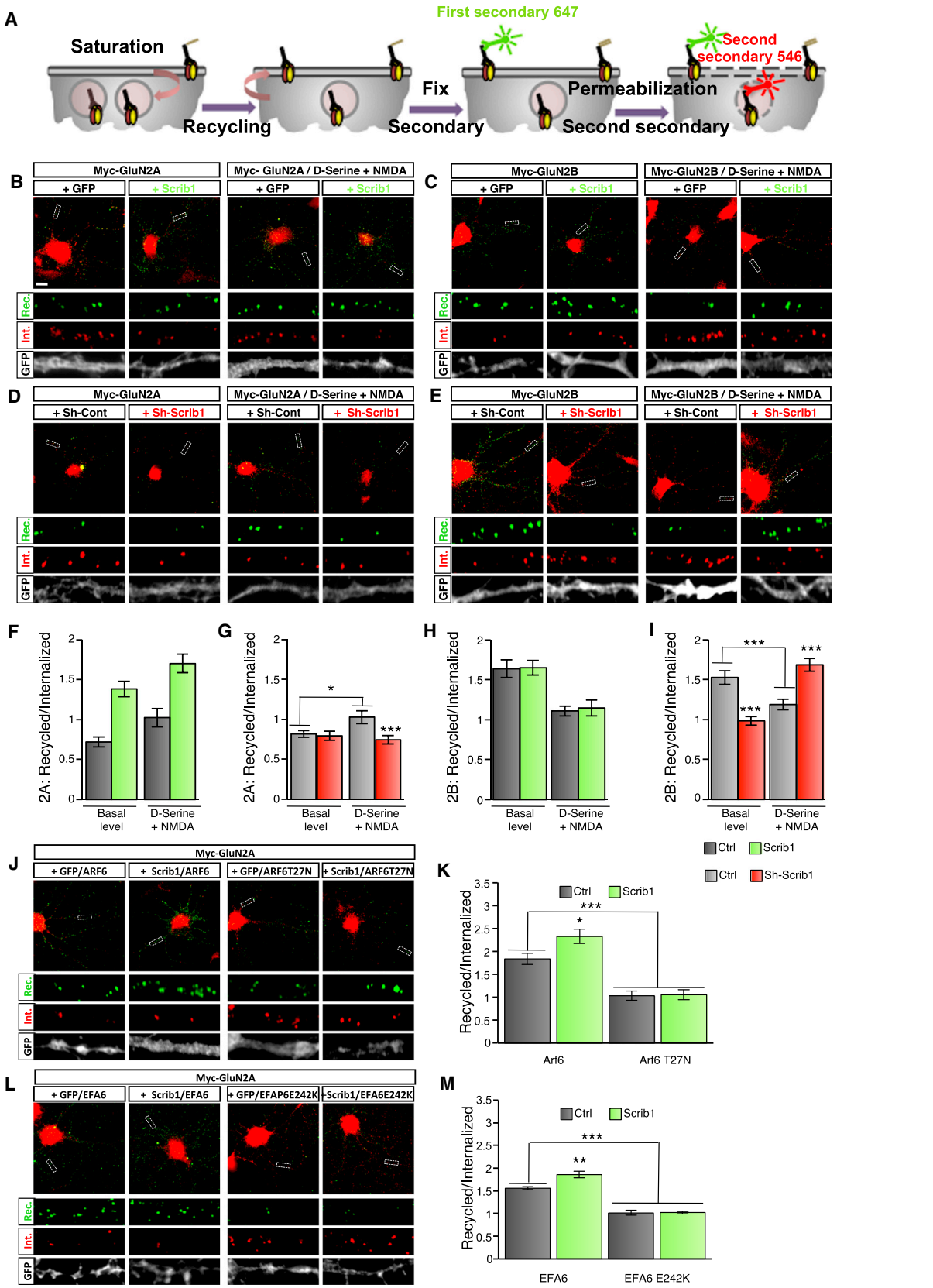

(legend on next page)

potential interacting site on Scrib1 fits in the classic binding site of AP2μ (Figures 6F–6H). In addition to the canonical Tyr834, several ionic bonds were observed (Arg839/Asp415, Glu838/Lys420, and Glu831/Arg357; Figure 6H). Notably, we identified a putative ionic bond between Glu838 and Lys420 at a position where there is typically a hydrophobic interaction, such as with residue Met204 from CTLA-4 (Follows et al., 2001). Our results suggest that the interaction of AP2 with Scrib1 uses a slightly different binding mode than the previously described associations with AP2μ. We further show that the internalizations of both GluN2A and GluN2B were reduced in the presence of a nonfunctional GFP-Scrib1^{Y834A} construct in hippocampal neurons (Figure 6I). These results show that a noncanonical, vertebrate-specific, endocytic motif in Scrib1 is recognized by the AP2 adaptors. Although Scrib1 does not change the internalization rate of GluN2A or GluN2B per se, binding of the AP2 adaptors to Scrib1 plays a role in the internalization (Figures 6I–6K) and likely in the subsequent recycling of NMDARs.

Scrib1 Regulates the Level of Synaptic NMDARs at Schaffer Collateral CA1 Pyramidal Cell Synapses

We performed single-cell electroporation of CA1 pyramidal cells in organotypic hippocampal slices with either pSUPER-shRNA-Scrib1 or pSUPER-shRNA-control. Three days after transfection, we recorded pharmacologically isolated NMDAR-mediated excitatory postsynaptic currents (EPSCs) from a transfected neuron and a neighboring nontransfected neuron in pairs (Figure 7A). Decreased levels of Scrib1 significantly reduced the amplitude of synaptic NMDAR-mediated responses compared to control (Figures 7B and 7C). The decay time of synaptic NMDAR-mediated EPSCs did not vary between the two conditions, suggesting that the acute downregulation of Scrib1 did not modify the composition of synaptic NMDARs (Figures 7B and 7C). On the other hand, in a similar experimental setting, overexpression of Scrib1 or GFP did not alter the amplitude or decay time of NMDAR-mediated EPSCs (Figure S7A). The reduction in the NMDAR-mediated EPSCs observed with the knockdown of Scrib1 could be mediated by the reduction in the number of synapses and not by a selective loss of NMDAR. To address this concern, we measured the α-amino-3-hydroxy-5-methyl-4-isoxazolepropionic acid (AMPA)/NMDA ratio in organotypic cultures. In our transfection time frame, we observed a change in the AMPA/NMDA ratio (Figure 7D). This imbalance can explain the decrease in NMDAR synaptic currents seen in Figure 7B. To further verify the selective effect on NMDAR, we measured the amplitude of pharmacologically isolated AMPA receptor (AMPAR)-mediated EPSCs and found that they were not different from controls when assessed with the paired recording experiment (Figures 7E and 7F). Our results confirm that Scrib1 downregulation affects specifically NMDAR currents with no major effect on AMPAR. The overexpression of Scrib1 did not cause any significant differences compared to control GFP (Figures S7B and S7C), suggesting that additional signals are necessary to drive the entry of GluN2A in synapses, as we have observed in Figure 2.

To confirm that the loss of Scrib1 does not alter the subunit composition of synaptic NMDARs, we tested the effect of Ro25-2981, a selective antagonist of NMDARs containing GluN2B. The effects of Ro25-2981 on the amplitude and decay time of NMDAR-mediated EPSCs in neurons transfected with pSUPER-shRNA-Scrib1 or with pSUPER-shRNA-control were not significantly different (Figure S7D) as compared to controls (Figure S7E). In conclusion, these data confirm that the loss of Scrib1 affects the levels of synaptic NMDARs in hippocampal excitatory synapses.

DISCUSSION

Here, we identified Scrib1 as a key PDZ protein involved in the functional and spatial regulation of synaptic NMDARs. First, we found a direct physical interaction between GluN2 subunits and Scrib1. Second, we demonstrated that Scrib1 levels modulate NMDAR trafficking and recycling to the membrane through a direct interaction with the AP2 adaptor proteins and the use of regulatory proteins, such as ARF6. Third, we showed that downregulation of Scrib1 in hippocampal neurons leads to a decrease in synaptic NMDAR currents.

NMDARs play a central role in controlling synaptic transmission and plasticity. Therefore, it has been a challenge to identify the molecular mechanisms that regulate GluN2A and GluN2B synaptic expression. In our previous study, we showed that, after 5 or 6 days posttransfection, the downregulation of Scrib1 in

Figure 5. Scrib1 Promotes GluN2A Recycling and Inhibits GluN2B Recycling upon Stimulation in Neuron Culture

(A) Timeline of the recycling experiments.

(B and C) Recycling of GluN2A- (B) and GluN2B- (C) containing NMDARs with or without stimulation. Overexpression of GFP-control or GFP-Scrib1 in primary hippocampal neuron culture transfected with myc-GluN2A (B) or myc-GluN2B (C) at 14 or 15 DIV.

(D and E) Recycling of GluN2A- (D) and GluN2B- (E) containing NMDARs with or without stimulation. Overexpression of sh-control or sh-Scrib1 in primary hippocampal neuron culture transfected with myc-GluN2A (D) or myc-GluN2B (E) at 14 or 15 DIV.

Recycling receptor populations are labeled in green, and internalized receptor populations are in red.

(F–I) Histograms represent the means of the ratio of recycled receptor puncta over internalized puncta corresponding, respectively, to the images in (B)–(E). (F) Data were compared using two-way ANOVA (n = 17 to 18 neurons). (G) Data were compared using two-way ANOVA and Bonferroni multiple comparison test (n = 13–15 neurons). (H) Data were compared using two-way ANOVA (n = 15–18 neurons). (I) Data were compared using two-way ANOVA and Bonferroni multiple comparison test (n = 15–20 neurons). Error bars are all ± SEM.

(J and K) Recycling of GluN2A-containing NMDARs with stimulation and overexpression of ARF6-HA, ARF6-DN-HA with GFP-control, or GFP-Scrib1 (J) and histograms represent the means of the ratio of recycled receptor puncta over internalized puncta (K). Data were compared using two-way ANOVA and Bonferroni multiple comparison test (n = 15–20 neurons) ± SEM. Error bars are all ± SEM.

(L and M) Recycling of GluN2A-containing NMDARs with stimulation and overexpression of EFA6-VSVG, EFA6-DN-VSVG with GFP-control, or GFP-Scrib1 (L) and histograms represent the means of the ratio of recycled receptor puncta over internalized puncta (M). Data were compared using two-way ANOVA and Bonferroni multiple comparison test (n = 10) ± SEM. Error bars are all ± SEM.

The scale bar represents 10 μm.

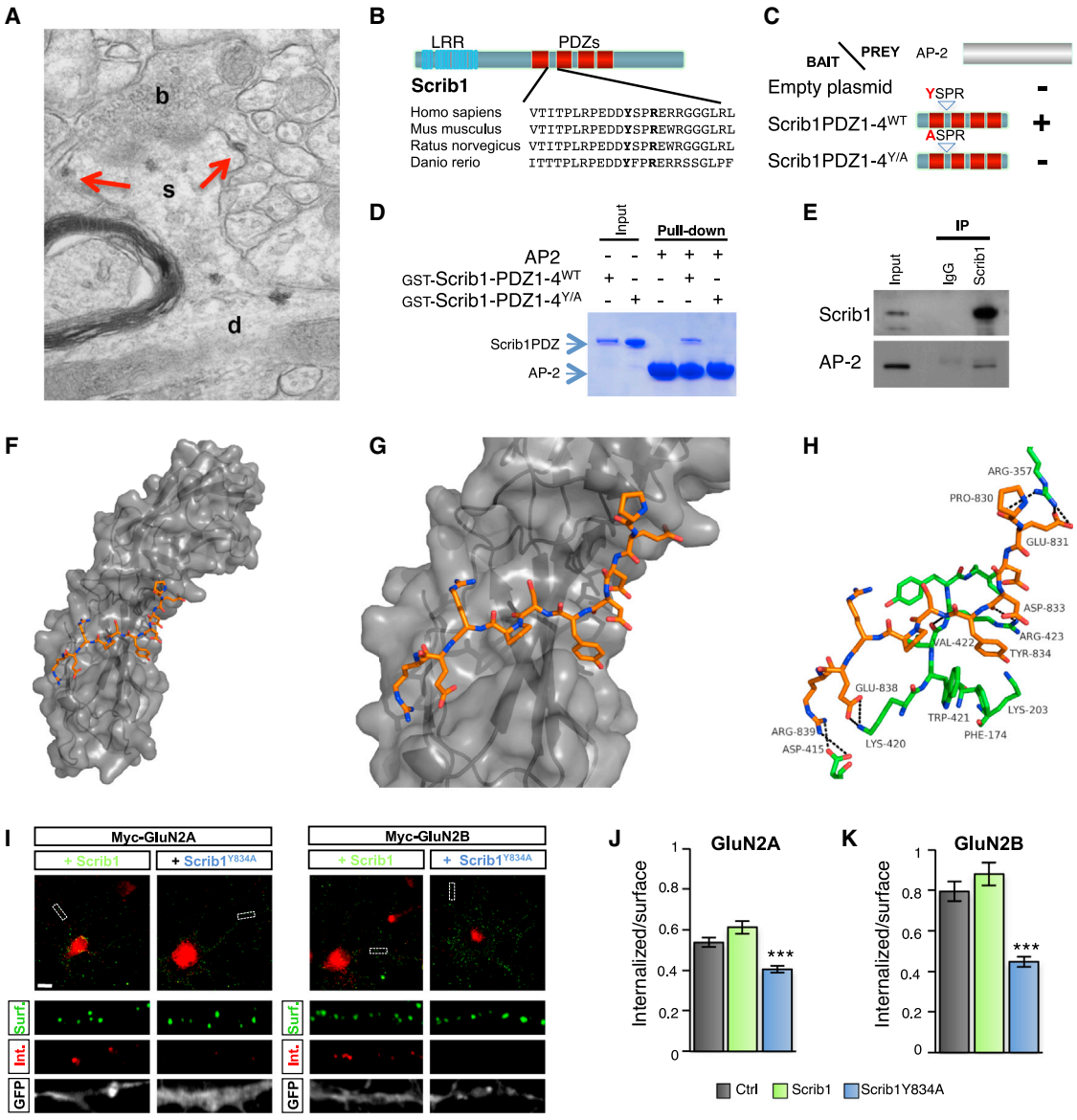

Figure 6. The Direct Interaction between Scrib1 and AP2 Is Necessary for Internalization of the Scribl1/GluN2 Complex

(A) Immunolabeling of Scrib1 in a dendritic spine in the CA1 stratum radiatum of the hippocampus. Electron microscopy image shows Scrib1 is found in the PSD and associated with the membrane of the spine (arrows). b, bouton; d, dendrite; s, spine.

(B) Schematic view of the Scrib1 YxxR motif, a conserved AP2 binding motif found between PDZ1 and PDZ2 of Scribble1.

(C) Directed yeast two-hybrid assays with AP2 fragment and Scrib1 PDZ constructs. Schematic of Scrib1 PDZ domain structures used as bait in yeast two-hybrid. Scrib1 binds AP2 via the YxxR binding domain site, and replacement of the lysine (Y) with an alanine (A; AxxR) disrupts this interaction. WT, wild-type.

(D) A pull-down assay indicates that AP2 binds to Scrib1 YxxR His-tagged protein, but not to mutated Scrib1 AxxR.

(E) Coimmunoprecipitation of endogenous Scrib1 and AP2 from the hippocampus. The lysates were immunoprecipitated with Scrib1 antibodies, and the precipitates were immunoblotted for AP2.

(F and G) Overall view of the model of the interaction between the binding region (gray) and the linker between PDZ1 and PDZ2 from Scrib1 (orange). Scrib1 residues 830–839 are represented as sticks, and AP2 is shown as a gray surface model.

(H) Stick model of the interactions of Phe174, Lys203, Arg357, Asp415, and Lys420 to Iso425 (green) with the Pro830 to Arg839 residues from the linker sequence between PDZ1 and PDZ2 from Scrib1 (orange).

(I) Internalization of GluN2A- and GluN2B-containing NMDARs. Myc-GluN2A and GFP-Scrib1 or GFP-Scrib1^{Y834A} (left panel) and Myc-GluN2B and GFP-Scrib1 or GFP-Scrib1^{Y834A} (right panel) were transfected into 14 or 15 DIV hippocampal neuron culture. The scale bar represents 10 μm.

(J and K) Histograms represent the means of the ratio of internalized receptor puncta over the surface receptor puncta ± SEM. (J) Data were compared using one-way ANOVA and Bonferroni multiple comparison test (n = 19 to 20 neurons). (K) Data were compared using one-way ANOVA and Bonferroni multiple comparison test (n = 15–18 neurons). Error bars are all ± SEM.

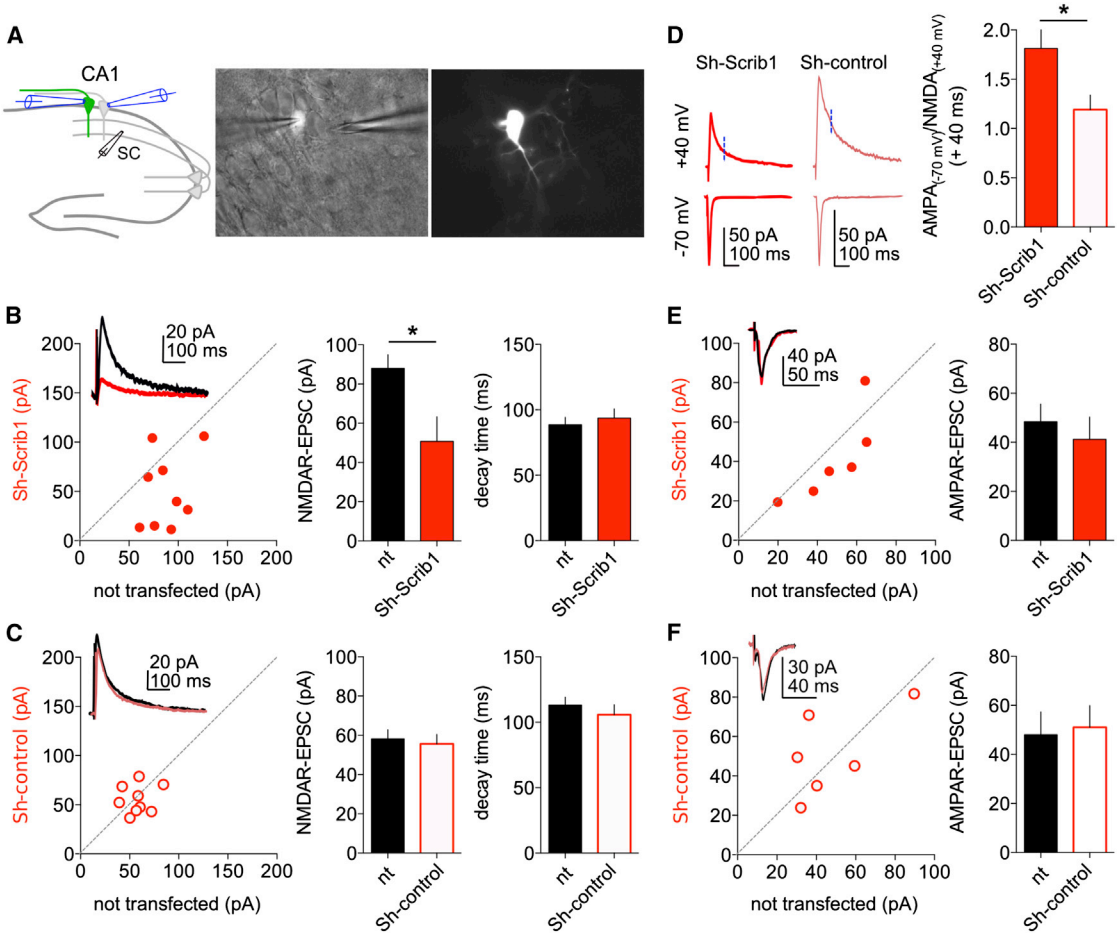

Figure 7. Scrib1 Regulates the Level of Synaptic NMDARs at Schaffer Collaterals CA1 Pyramidal Cells Synapse

(A) Schematic cartoon illustrating paired recordings from neighboring electroporated and not electroporated (control) neurons in CA1 pyramidal layer. Whole-cell voltage-clamp recordings were performed at +40 mV while stimulating the Schaffer collaterals (SC) every 10 s. On the right, example images of a pair of recorded neighboring neurons.

(B) Transfection with pSUPER-shRNA-Scrib1 reduces the amplitude of NMDAR-mediates EPSCs at SC-CA1 synapse but does not modify their decay time. Sample traces shown in the inset (control: n = 9; pSUPER-shRNA-Scrib1: n = 9). nt, not transfected.

(C) pSUPER-shRNA-control transfection does not affect the NMDAR-mediates EPSCs at SC-CA1 synapse (amplitude and decay time); sample traces shown in the inset (control: n = 9; pSUPER-shRNA-control: n = 9).

(D) Sample traces and summary graphs illustrating transfection of pSUPER-shRNA-Scrib1 induces a significant change in the AMPA/NMDA ratio when compared to cells transfected with pSUPER-shRNA-control inset (pSUPER-shRNA-Scrib1: n = 10; pSUPER-shRNA-control: n = 11).

(E) Transfection with pSUPER-shRNA-Scrib1 does not modify the amplitude of AMPAR-mediates EPSCs at SC-CA1 synapse (control: n = 6; pSUPER-shRNA-Scrib1: n = 6).

(F) Transfection with pSUPER-shRNA-control does not modify the amplitude of AMPAR-mediates EPSCs at SC-CA1 synapse (control: n = 6; pSUPER-shRNA-control: n = 6).

dissociated hippocampal resulted in a decrease in spine density (Moreau et al., 2010). In the present study, we studied the early effect of Scrib1 loss on NMDAR trafficking, with a reduced post-transfection delay and processing of 48 hr. This shorter time was carefully chosen to minimize spine loss while still having a down-regulation of Scrib1 protein above 70%. The unchanged synaptophysin puncta density after 48 hr posttransfection supports our claim of an absence of massive loss of synapses. Under these experimental conditions, we were able to reveal specific effects of Scrib1 levels on NMDAR trafficking. Our results suggest that the first effect of Scrib1 knockdown in hippocampal neurons is the decreased levels of GluN2A and GluN2B at the membrane, with a difference in the endocytosis or recycling rates of the two subunits. These differential effects of Scrib1 levels on GluN2A versus GluN2B endocytosis and recycling are consistent with previously observed differences in GluN2A and GluN2B secretory trafficking (Roche et al., 2001; Lavezzari et al., 2004). We showed that this Scrib1-dependent regulation of GluN2A and GluN2B endocytosis and recycling is specific because β3-containing $GABA_A$ receptors are not affected under the same conditions. Moreover, 3 days after transfection of shRNA for Scrib1 in organotypic slice cultures, the loss of Scrib1

in CA1 neurons decreased the amplitude of NMDAR-synaptic currents, but not of AMPAR-EPSCs, supporting the idea that Scrib1 regulates the number of NMDARs present at synapses. The changes in the surface expression of NMDARs could result from either impaired exocytosis of novel receptors or enhanced endocytosis followed by an impaired exocytosis of recycled receptors. Similar effects to Scrib1 on trafficking were also observed for G-protein-coupled receptor thyrotropin receptors (Lahuna et al., 2005) and integrin α5 (Michaelis et al., 2013). This impairment in recycling is presumably due to a failure of the normal recycling pathway in early endosomes that contain GluN2 but lack Scrib1, thus driving the receptors to the late lysosomal compartment. Scrib1 colocalizes strongly with Rab5a and Rab11 in early and recycling endosomes, respectively, suggesting that Scrib1 has a dynamic function in endocytosis and the recycling of NMDARs. Scrib1 is likely to interact with components of the membrane fusion machinery involved in the recycling of NMDARs. Consistent with this, we found that Sec8, a member of the exocyst complex, interacts with Scrib1 in the hippocampus (N.H.P. and N.S., data not shown). It is known that the exocyst complex and ARF6 control postendocytic recycling (Prigent et al., 2003) and that Scrib1 signaling involves ARF6 (Lahuna et al., 2005). Our own data show that ARF6^{T27N} or EFA6^{E242K} constructs both block GluN2A recycling, implicating the ARF6 pathway in the regulation of NMDARs. This is also consistent with previous studies showing that SNAP23 or SNAP25 regulate NMDAR trafficking by acting as a component of the membrane fusion machinery and not by directly binding NMDAR (Lau et al., 2010; Suh et al., 2010). Electron microscopy analysis showed that Scrib1 colocalizes with NMDARs and is often localized to the lateral domain of the spine, where activity-dependent exocytosis and endocytosis domains are present (Kennedy and Ehlers, 2006). Moreover, it has been shown that Scrib1 can form a complex with syntaxin 4 (Massimi et al., 2008), one of the target-membrane-associated SNARE involved in spine exocytosis (Kennedy et al., 2010). We thus favor a model whereby Scrib1 facilitates AP2-dependent internalization of NMDAR and then associates with syntaxin to drive recycling of NMDAR-containing endocytic compartments back to the membrane, probably through a SNARE/exocyst complex.

After the priming of the receptors by D-serine stimulation, the major NMDAR coagonist at the synapse (Papouin et al., 2012), AP2 either binds directly to the NMDARs and drives them to the degradation pathway or binds to Scrib1 and initiates endocytosis and recycling of the NMDAR/Scrib1 complex. Moreover, D-serine stimulation prior to D-serine/NMDA activation affects differently the pool of surface GluN2A and GluN2B. Further work is needed to understand the molecular mechanism underlying the differences upon D-serine stimulation described in this study.

Interestingly, we show that the overexpression of a Scrib1-AP2 binding-defective mutant (Scrib1^{Y834A}) reduces both GluN2A and GluN2B internalization (Figure 6J) whereas Scrib1 shRNA has the opposite effect (Figures 5G and 5I). This differential effect of Scrib1 knockdown versus ectopic expression reveals presumably a dominant-negative role of Scrib1^{Y834A}. The sh-Scrib1 experiments reveal the effect of the absence of Scrib1 on GluN2A and GluN2B receptors. Indeed, we showed that GluN2A endocytosis increases in absence of Scrib1 expression. We believe this emphasizes the role of Scrib1 on the stabilization of GluN2A at the membrane. Hence, in absence of Scrib1, GluN2A is less stable, and nothing prevents the direct binding of AP2 to the subunit and its internalization (Lavezzari et al., 2004). On the contrary, GluN2B endocytosis decreases in absence of Scrib1 expression, supporting an active role for Scrib1 in the endocytosis process, but not in the stabilization of the GluN2B subunit. In presence of Scrib1^{Y834A} mutant, both GluN2A and GluN2B endocytosis is reduced, revealing the dependence of each subunit on the AP2 binding motif of Scrib1 for endocytosis. Here, the mutated Scrib1 can still bind the subunits via the PDZ domains and fulfil some of its function: stabilization for GluN2A and blocking of the internalization for GluN2B. However, the mutation of the AP2 motif on Scrib1^{Y834A} partially affects some of Scrib1 downstream effects, revealing an AP2-dependent mechanism in NMDAR-induced internalization via Scrib1. Only one previous study has described a direct interaction between a cytoplasmic cargo protein and the μ-adaptin subunits during membrane receptor internalization. In Yu et al. (2007), the authors showed that the planar cell polarity protein Dishevelled associates with AP2 to induce the endocytosis of Frizzled coupled to its degradation (Yu et al., 2007). Interestingly, Scrib1, which is also a planar cell polarity protein, couples the internalization of the receptors to recycling.

We found that the interaction between GluN2 and Scrib1 is mediated by the carboxy-terminal PDZ-BD of GluN2 and the Scrib1 PDZ domains 2 and 3 because a Scrib1 form lacking these two domains has no influence on NMDAR trafficking. NMDARs have been shown to bind numerous PDZ proteins, including all four members of the PSD-95 family of MAGUKs (PSD-95, SAP102, PSD-93, and SAP97), MAGI1–MAGI3, MALS1–MALS3, CIPP, and GIPC (Wenthold et al., 2003; Yi et al., 2007); several of these proteins play roles in anchoring the receptors (Roche et al., 2001; Sans et al., 2000) and likely compete with Scrib1 for NMDAR binding. Various studies have shown that AP2 binds directly to NMDARs (Prybylowski et al., 2005; Scott et al., 2004) and that, after direct binding to AP2, GluN2A or GluN2B are degraded, except when AP2 binds the YEKL motif near the PDZ-BD of GluN2B (Scott et al., 2004). We and others have shown that Fyn kinase or hippocalcin can cause the dissociation of PSD-95 from NMDARs, allowing AP2 to bind to the receptors, thus inducing their internalization (Jo et al., 2010; Prybylowski et al., 2005). Our model shows that Scrib1 can stabilize GluN2A-containing NMDARs in basal conditions, whereas upon activation, Scrib1 leads to the entry of GluN2A-containing NMDARs into the recycling pathway. In contrast, Scrib1 plays a role in GluN2B-containing NMDAR trafficking by preventing their recycling upon stimulation. These different mechanisms maintain the GluN2A/GluN2B ratio in basal conditions and mediate the switch from surface GluN2B to GluN2A, leading to an increased GluN2A/GluN2B ratio upon stimulation. The fact that GluN2A can be recycled in the presence of Scrib1 after the activation of NMDARs is consistent with the concept that the activation pathways of distinct NMDARs use different scaffold and adaptor complexes for proper intracellular traffic and regulation. It is also possible that Scrib1 participates in the direct sorting of NMDAR. Our data using a mutated form of Scrib1 missing the two PDZ domains seem to argue against

the latter hypothesis (Figures 3A–3F), but additional experiments will be needed to answer this question.

We showed that, in the presence of Scrib1, GluN2A can recycle back to the membrane, and thus GluN2B is not the only NMDAR subunit that can recycle. This dual mechanism has been known for a long time for AMPARs. It has been demonstrated quite convincingly that activation of NMDAR triggers internalization and recycling of GluA1-containing AMPARs and that GluA2 and GluA2/GluA3 constitutively recycle (Barry and Ziff, 2002; Ehlers, 2000; Henley et al., 2011; Shepherd and Huganir, 2007). It will be important for future studies to assess the specific consequences of the recycling of GluN2A on AMPAR trafficking at synapses.

Together, our results show that Scrib1 is a key scaffolding molecule regulated by activity in vivo and in vitro and that it is responsible for the internalization and recycling of NMDA receptors. Together with recent publications (Groc et al., 2006; Prybylowski et al., 2005; Suh et al., 2010), our work strengthens the emerging idea that different PDZ proteins regulate GluR trafficking at the membrane via the endosomal system. This mechanism involving Scrib1 is likely to be implicated in the regulation of synapse function in numerous physiological processes and pathological states that involve interactions between NMDARs, Scrib1, and AP2.

EXPERIMENTAL PROCEDURES

Animals

All rats were Sprague-Dawley between embryonic day 18 (E18) and 10 weeks old at the time of experiments. Rats had free access to food and water and were housed in polypropylene cages under controlled conditions (at 23°C ± 1°C, with lights on from 7:00 a.m. to 7:00 p.m,, assuring a 12:12 hr light/dark cycle), with the behavioral testing or the other experiments performed during the light portion of the cycle. All procedures were performed according to the requirements of the United Kingdom Animals (Scientific Procedures) Act 1986, AWERB Newcastle University (ID: 374), the European Communities Council Directives (86/609/EEC), and the French National Committee (87/848) recommendations.

Antibodies and Vector Constructions

The detailed information on antibodies and constructs used in this study are in the Supplemental Experimental Procedures.

Yeast Two-Hybrid Assays

pGBKT7-GluN2A and pGBKT7-GluN2B were used as described previously (Yi et al., 2007). Scrib1^{PDZ} (amino acids 712–1,187 of the Q80U72-3 sequence) was subcloned into pGAD and pGBTK7 and modified by site-directed mutagenesis (Stratagen). Yeast two-hybrid screening was performed only once with the library, and yeast assays to confirm the interaction were performed at least three times as described in the Clontech protocol.

Detergent Solubilization and Immunoprecipitation Experiment

IP experiments were performed after 1% sodium deoxycholate, 0.1% Triton X-100 solubilization as described previously (Sans et al., 2003).

Culture and Transfections of Hippocampal Neurons

Primary hippocampal cultures were prepared from E18 Sprague-Dawley rats. Cultures were transfected with the different constructs at 12 or 14 days in culture using the calcium phosphate method (Moreau et al., 2010; Sans et al., 2005).

Surface, Internalization, and Recycling Experiments in Neurons

Hippocampal neurons (12 days in vitro [DIV]) were transfected with GFP control or GFP-Scrib1; control shRNA or Scrib1 shRNA; or myc-tagged GluN2A, GluN2B, or GABA$_A$ β3 using calcium phosphate methods (Sans et al., 2003). The experiments were performed 36–48 hr after transfection. The protocol to measure recycled NMDARs after internalization in hippocampal neurons was adapted from previous studies (Suh et al., 2010). The stimulation was adapted from Nong et al. (2003). Briefly, prestimulation with D-serine (100 μM) was performed for 5 min followed by a stimulation with NMDA (50 μM) plus D-serine (1 μM) over 5 min before the internalization step. See also the Supplemental Experimental Procedures.

Data Presentation and Statistical Analysis

The results are described as mean ± SEM or whiskers boxes. Two-way ANOVA, one-way ANOVA, or Kruskal-Wallis one way was performed where indicated. For most experiments, the Student's t test was used to determine statistical significance (*$p < 0.05$; **$p < 0.01$; ***$p < 0.001$). Statistical analyses were performed using the Statistica or GraphPad Prism statistical package (GraphPad). See also the Supplemental Experimental Procedures and Table S2.

Additional Methods

Details regarding the methods used for ITC, pull-down assays; fractionation; culture and transfections of HEK293 or COS-7 cells; surface, internalization, and recycling experiments in fibroblasts and neurons; pre-embedding immunocytochemistry or postembedding immunogold; electrophysiological recordings in slice; and data analysis are provided in the Supplemental Experimental Procedures.

SUPPLEMENTAL INFORMATION

Supplemental Information includes Supplemental Experimental Procedures, seven figures, and two tables and can be found with this article online at http://dx.doi.org/10.1016/j.celrep.2014.09.017.

ACKNOWLEDGMENTS

We thank M.C. Donat, D. Arma, E. Richard, and Y.-X. Wang for technical assistance. We thank I. Macara for the GFP-Scrib constructs, J.P. Borg for the Lano and Erbin antibodies and the HA-Scrib1 construct, K. Roche for supplying the Tac constructs, T. Galli for the CD63 cDNA, P.D. Stahl for the Rab5 cDNAs, F. Luton for the EFA6 mutated construct, G. Köhr for the GluN monoclonal antibodies, and M. Garret for supplying the β3 cDNA and antibody. We also thank the Biochemistry and Biophysics Facility of the Bordeaux Neurocampus funded by the Labex BRAIN (ANR-10-LABX-43), the Sequencing facility (Bordeaux University), and the Electron Microscopy Research Services (Faculty of Medical Sciences, Newcastle University). This work was supported by INSERM and INSERM AVENIR grants to N.S. and M.M., Conseil Régional d'Aquitaine (to N.S. and M.M.), Neurocampus program (to M.M.), La Fondation pour la Recherche Médicale (to N.S. and M.M.), ANR NeuroScrib ANR-07-NEUR-031-01 (to N.S. and M.M.), ANR MossyPCP ANR-12-BSV4-0016-01 (to N.S. and C. Mulle), Conseil Régional d'Aquitaine/INSERM Ph.D. fellowship and FRM Bourse de soudure fellowship (to N.P.), the Cifre Program (to J.-M.B.), the European ITN SyMBaD and FRM 4eme année de these FDT20130928124 (to V.L.P.), FRM fellowships SPF20081215186 (to C.M.D.), BioXtal SARL (to L.V.), Royal Society International Joint Project grant (to C.R. and N.S.), and the Wellcome Trust Institutional Strategic Support Fund Project, Faculty of Medical Sciences, Newcastle University (to C.R.). K.C., R.S.P., and R.J.W. were supported by the Intramural Research Program of NIDCD/NIH. The M.M. and N.S. and the C.M. labs are members of the Labex BRAIN.

Received: October 3, 2013
Revised: June 18, 2014
Accepted: September 9, 2014
Published: October 9, 2014

REFERENCES

Barria, A., and Malinow, R. (2002). Subunit-specific NMDA receptor trafficking to synapses. Neuron *35*, 345–353.

Barry, M.F., and Ziff, E.B. (2002). Receptor trafficking and the plasticity of excitatory synapses. Curr. Opin. Neurobiol. *12*, 279–286.

Chung, H.J., Huang, Y.H., Lau, L.F., and Huganir, R.L. (2004). Regulation of the NMDA receptor complex and trafficking by activity-dependent phosphorylation of the NR2B subunit PDZ ligand. J. Neurosci. *24*, 10248–10259.

Ehlers, M.D. (2000). Reinsertion or degradation of AMPA receptors determined by activity-dependent endocytic sorting. Neuron *28*, 511–525.

Elias, G.M., and Nicoll, R.A. (2007). Synaptic trafficking of glutamate receptors by MAGUK scaffolding proteins. Trends Cell Biol. *17*, 343–352.

Follows, E.R., McPheat, J.C., Minshull, C., Moore, N.C., Pauptit, R.A., Rowsell, S., Stacey, C.L., Stanway, J.J., Taylor, I.W., and Abbott, W.M. (2001). Study of the interaction of the medium chain mu 2 subunit of the clathrin-associated adapter protein complex 2 with cytotoxic T-lymphocyte antigen 4 and CD28. Biochem. J. *359*, 427–434.

Franco, M., Peters, P.J., Boretto, J., van Donselaar, E., Neri, A., D'Souza-Schorey, C., and Chavrier, P. (1999). EFA6, a sec7 domain-containing exchange factor for ARF6, coordinates membrane recycling and actin cytoskeleton organization. EMBO J. *18*, 1480–1491.

Groc, L., Heine, M., Cousins, S.L., Stephenson, F.A., Lounis, B., Cognet, L., and Choquet, D. (2006). NMDA receptor surface mobility depends on NR2A-2B subunits. Proc. Natl. Acad. Sci. USA *103*, 18769–18774.

Groc, L., Bard, L., and Choquet, D. (2009). Surface trafficking of N-methyl-D-aspartate receptors: physiological and pathological perspectives. Neuroscience *158*, 4–18.

Henley, J.M., Barker, E.A., and Glebov, O.O. (2011). Routes, destinations and delays: recent advances in AMPA receptor trafficking. Trends Neurosci. *34*, 258–268.

Howard, M.A., Elias, G.M., Elias, L.A., Swat, W., and Nicoll, R.A. (2010). The role of SAP97 in synaptic glutamate receptor dynamics. Proc. Natl. Acad. Sci. USA *107*, 3805–3810.

Jo, J., Son, G.H., Winters, B.L., Kim, M.J., Whitcomb, D.J., Dickinson, B.A., Lee, Y.B., Futai, K., Amici, M., Sheng, M., et al. (2010). Muscarinic receptors induce LTD of NMDAR EPSCs via a mechanism involving hippocalcin, AP2 and PSD-95. Nat. Neurosci. *13*, 1216–1224.

Jurd, R., Thornton, C., Wang, J., Luong, K., Phamluong, K., Kharazia, V., Gibb, S.L., and Ron, D. (2008). Mind bomb-2 is an E3 ligase that ubiquitinates the N-methyl-D-aspartate receptor NR2B subunit in a phosphorylation-dependent manner. J. Biol. Chem. *283*, 301–310.

Kennedy, M.J., and Ehlers, M.D. (2006). Organelles and trafficking machinery for postsynaptic plasticity. Annu. Rev. Neurosci. *29*, 325–362.

Kennedy, M.J., Davison, I.G., Robinson, C.G., and Ehlers, M.D. (2010). Syntaxin-4 defines a domain for activity-dependent exocytosis in dendritic spines. Cell *141*, 524–535.

Lahuna, O., Quellari, M., Achard, C., Nola, S., Méduri, G., Navarro, C., Vitale, N., Borg, J.P., and Misrahi, M. (2005). Thyrotropin receptor trafficking relies on the hScrib-betaPIX-GIT1-ARF6 pathway. EMBO J. *24*, 1364–1374.

Lau, C.G., and Zukin, R.S. (2007). NMDA receptor trafficking in synaptic plasticity and neuropsychiatric disorders. Nat. Rev. Neurosci. *8*, 413–426.

Lau, C.G., Takayasu, Y., Rodenas-Ruano, A., Paternain, A.V., Lerma, J., Bennett, M.V., and Zukin, R.S. (2010). SNAP-25 is a target of protein kinase C phosphorylation critical to NMDA receptor trafficking. J. Neurosci. *30*, 242–254.

Lavezzari, G., McCallum, J., Dewey, C.M., and Roche, K.W. (2004). Subunit-specific regulation of NMDA receptor endocytosis. J. Neurosci. *24*, 6383–6391.

Losi, G., Prybylowski, K., Fu, Z., Luo, J., Wenthold, R.J., and Vicini, S. (2003). PSD-95 regulates NMDA receptors in developing cerebellar granule neurons of the rat. J. Physiol. *548*, 21–29.

Massimi, P., Narayan, N., Thomas, M., Gammoh, N., Strand, S., Strand, D., and Banks, L. (2008). Regulation of the hDlg/hScrib/Hugl-1 tumour suppressor complex. Exp. Cell Res. *314*, 3306–3317.

Mauceri, D., Gardoni, F., Marcello, E., and Di Luca, M. (2007). Dual role of CaMKII-dependent SAP97 phosphorylation in mediating trafficking and insertion of NMDA receptor subunit NR2A. J. Neurochem. *100*, 1032–1046.

Michaelis, U.R., Chavakis, E., Kruse, C., Jungblut, B., Kaluza, D., Wandzioch, K., Manavski, Y., Heide, H., Santoni, M.J., Potente, M., et al. (2013). The polarity protein Scrib is essential for directed endothelial cell migration. Circ. Res. *112*, 924–934.

Montgomery, J.M., Selcher, J.C., Hanson, J.E., and Madison, D.V. (2005). Dynamin-dependent NMDAR endocytosis during LTD and its dependence on synaptic state. BMC Neurosci. *6*, 48.

Moreau, M.M., Piguel, N., Papouin, T., Koehl, M., Durand, C.M., Rubio, M.E., Loll, F., Richard, E.M., Mazzocco, C., Racca, C., et al. (2010). The planar polarity protein Scribble1 is essential for neuronal plasticity and brain function. J. Neurosci. *30*, 9738–9752.

Nong, Y., Huang, Y.Q., Ju, W., Kalia, L.V., Ahmadian, G., Wang, Y.T., and Salter, M.W. (2003). Glycine binding primes NMDA receptor internalization. Nature *422*, 302–307.

Papouin, T., Ladépêche, L., Ruel, J., Sacchi, S., Labasque, M., Hanini, M., Groc, L., Pollegioni, L., Mothet, J.P., and Oliet, S.H. (2012). Synaptic and extrasynaptic NMDA receptors are gated by different endogenous coagonists. Cell *150*, 633–646.

Pérez-Otaño, I., Luján, R., Tavalin, S.J., Plomann, M., Modregger, J., Liu, X.B., Jones, E.G., Heinemann, S.F., Lo, D.C., and Ehlers, M.D. (2006). Endocytosis and synaptic removal of NR3A-containing NMDA receptors by PACSIN1/syndapin1. Nat. Neurosci. *9*, 611–621.

Prigent, M., Dubois, T., Raposo, G., Derrien, V., Tenza, D., Rossé, C., Camonis, J., and Chavrier, P. (2003). ARF6 controls post-endocytic recycling through its downstream exocyst complex effector. J. Cell Biol. *163*, 1111–1121.

Prybylowski, K., Chang, K., Sans, N., Kan, L., Vicini, S., and Wenthold, R.J. (2005). The synaptic localization of NR2B-containing NMDA receptors is controlled by interactions with PDZ proteins and AP-2. Neuron *47*, 845–857.

Roche, K.W., Standley, S., McCallum, J., Dune Ly, C., Ehlers, M.D., and Wenthold, R.J. (2001). Molecular determinants of NMDA receptor internalization. Nat. Neurosci. *4*, 794–802.

Sans, N., Petralia, R.S., Wang, Y.X., Blahos, J., 2nd, Hell, J.W., and Wenthold, R.J. (2000). A developmental change in NMDA receptor-associated proteins at hippocampal synapses. J. Neurosci. *20*, 1260–1271.

Sans, N., Prybylowski, K., Petralia, R.S., Chang, K., Wang, Y.X., Racca, C., Vicini, S., and Wenthold, R.J. (2003). NMDA receptor trafficking through an interaction between PDZ proteins and the exocyst complex. Nat. Cell Biol. *5*, 520–530.

Sans, N., Wang, P.Y., Du, Q., Petralia, R.S., Wang, Y.X., Nakka, S., Blumer, J.B., Macara, I.G., and Wenthold, R.J. (2005). mPins modulates PSD-95 and SAP102 trafficking and influences NMDA receptor surface expression. Nat. Cell Biol. *7*, 1179–1190.

Sanz-Clemente, A., Matta, J.A., Isaac, J.T., and Roche, K.W. (2010). Casein kinase 2 regulates the NR2 subunit composition of synaptic NMDA receptors. Neuron *67*, 984–996.

Sanz-Clemente, A., Gray, J.A., Ogilvie, K.A., Nicoll, R.A., and Roche, K.W. (2013). Activated CaMKII couples GluN2B and casein kinase 2 to control synaptic NMDA receptors. Cell Reports *3*, 607–614.

Scott, D.B., Michailidis, I., Mu, Y., Logothetis, D., and Ehlers, M.D. (2004). Endocytosis and degradative sorting of NMDA receptors by conserved membrane-proximal signals. J. Neurosci. *24*, 7096–7109.

Sheng, M., and Hoogenraad, C.C. (2007). The postsynaptic architecture of excitatory synapses: a more quantitative view. Annu. Rev. Biochem. *76*, 823–847.

Shepherd, J.D., and Huganir, R.L. (2007). The cell biology of synaptic plasticity: AMPA receptor trafficking. Annu. Rev. Cell Dev. Biol. *23*, 613–643.

Suh, Y.H., Terashima, A., Petralia, R.S., Wenthold, R.J., Isaac, J.T., Roche, K.W., and Roche, P.A. (2010). A neuronal role for SNAP-23 in postsynaptic glutamate receptor trafficking. Nat. Neurosci. *13*, 338–343.

Traub, L.M. (2009). Tickets to ride: selecting cargo for clathrin-regulated internalization. Nat. Rev. Mol. Cell Biol. *10*, 583–596.

Traynelis, S.F., Wollmuth, L.P., McBain, C.J., Menniti, F.S., Vance, K.M., Ogden, K.K., Hansen, K.B., Yuan, H., Myers, S.J., and Dingledine, R. (2010). Glutamate receptor ion channels: structure, regulation, and function. Pharmacol. Rev. *62*, 405–496.

Uekita, T., Itoh, Y., Yana, I., Ohno, H., and Seiki, M. (2001). Cytoplasmic tail-dependent internalization of membrane-type 1 matrix metalloproteinase is important for its invasion-promoting activity. J. Cell Biol. *155*, 1345–1356.

Wenthold, R.J., Prybylowski, K., Standley, S., Sans, N., and Petralia, R.S. (2003). Trafficking of NMDA receptors. Annu. Rev. Pharmacol. Toxicol. *43*, 335–358.

Yashiro, K., and Philpot, B.D. (2008). Regulation of NMDA receptor subunit expression and its implications for LTD, LTP, and metaplasticity. Neuropharmacology *55*, 1081–1094.

Yi, Z., Petralia, R.S., Fu, Z., Swanwick, C.C., Wang, Y.X., Prybylowski, K., Sans, N., Vicini, S., and Wenthold, R.J. (2007). The role of the PDZ protein GIPC in regulating NMDA receptor trafficking. J. Neurosci. *27*, 11663–11675.

Yu, A., Rual, J.F., Tamai, K., Harada, Y., Vidal, M., He, X., and Kirchhausen, T. (2007). Association of Dishevelled with the clathrin AP-2 adaptor is required for Frizzled endocytosis and planar cell polarity signaling. Dev. Cell *12*, 129–141.

Cell Reports, Volume *9*

Supplemental Information

Scribble1/AP2 Complex Coordinates NMDA Receptor Endocytic Recycling

Nicolas H. Piguel, Sabine Fievre, Jean-Michel Blanc, Mario Carta, Maïté M. Moreau, Enora Moutin, Vera L. Pinheiro, Chantal Medina, Jerome Ezan, Léa Lasvaux, François Loll, Christelle M. Durand, Kai Chang, Ronald S. Petralia, Robert J. Wenthold, F. Anne Stephenson, Laurent Vuillard, Hervé Darbon, Julie Perroy, Christophe Mulle, Mireille Montcouquiol, Claudia Racca, and Nathalie Sans

Inventory of Supplemental Informations:

Supplemental informations include eight supplemental figures (Figures S1–S8), two supplemental tables (Tables S1 and S2), one file with supplemental experimental procedures and supplemental references.

Figure S1. Scribble1 expression at synapses and in vesicles. Related to Figure 1.

Figure S2. Scrib1 levels affect the surface expression of myc-GluN2A- and myc-GluN2B-containing receptors. Related to Figure 3.

Figure S3. Scrib1 levels affect the surface expression of GluN2A- and GluN2B-containing receptors after stimulation. Related to Figure 3.

Figure S4. Co-expression of Scrib1, Tac-GluN2A or Tac-GluN2B and endosomal markers in heterologous cells. Related to Figure 4 and Figure 5.

Figure S5. Overexpression of Scrib1 modifies GluN2A receptors endocytic sorting. Related to Figure 5.

Figure S6. Down regulation of Scrib1 modifies differentially GluN2A and GluN2B-containing receptors endocytic sorting. Related to Figure 5.

Figure S7. Overexpression of Scrib1 does not regulate the level of NMDARs at Schaffer collaterals CA1 pyramidal cells synapse. Related to Figure 7.

Table S1. Thermodynamic Binding Parameters for Scrib1 PDZ domains and GluN2A or GluN2B peptides determined by ITC. Related to Figure 1.

Table S2. Statistics reporting, by figure.

Supplemental experimental procedures.

Supplemental references.

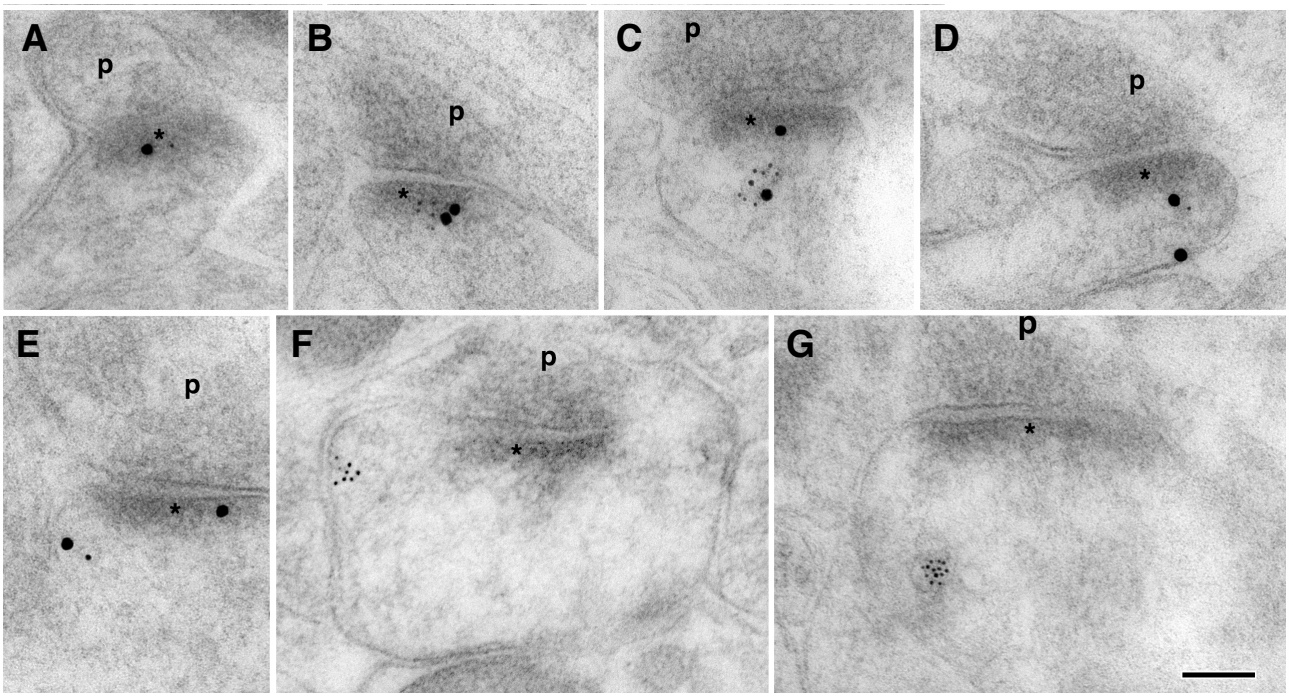

Figure S1. Scribble1 expression at synapses and in vesicles. Related to Figure 1.

(**A,E**) Immunogold localization of Scrib1 (5 nm) and its colocalization with GluN1 (15 nm) in hippocampal CA1 stratum radiatum synapses. Asterisk, postsynaptic density; p, presynaptic terminal. Note the double labelling at the synapse (A-B) as well as in a vesicle in the spine cytoplasm (C-E).
(**F,G**) The bottom two images show labelling for Scrib1 at the extrasynaptic membrane (F) and in a cytoplasmic vesicle (G). Scale bar, 100 nm.

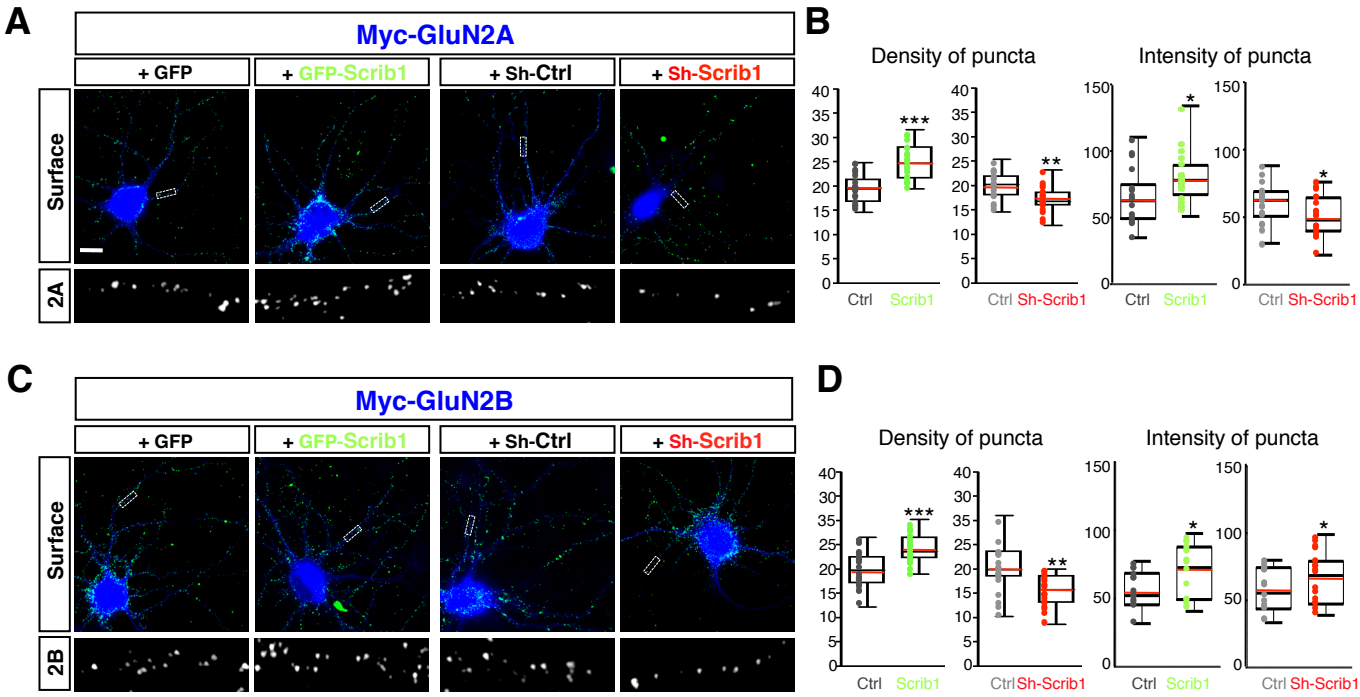

Figure S2. Scrib1 levels affect the surface expression of myc-GluN2A- and myc-GluN2B-containing receptors. Related to Figure 3.

(**A,C**) The surface expression of myc-GluN2A- (A) and myc-GluN2B-containing NMDARs (C). Overexpression of GFP-control, GFP-Scrib1, Sh-Control or Sh-Scrib1 in primary hippocampal neuron cultures transfected with myc-GluN2A (A) or myc-GluN2B (C) at 14 to 15 DIV. Surface receptor populations are labelled in green (scale bar = 10µm).

(**B, D**) Box-and-whisker plots indicate the median value (black line) and mean value (red line), the 25-75th (box) and the 10-90th (whiskers); open circles represent individual values for puncta number or intensity (n = 20 from at least 3 experiments). (B) Data were compared using Unpaired t test (*p<0.05, **p<0.01, ***p<0.001). Density for Scrib1: t(38)=3.811, p<0.001 and ShScrib1: t(38)=3.063, p=0.004; Intensity for Scrib1: t(38)=2.31, p=0.023 and ShScrib1: t(38)=2.276, p=0.029. (D) Data were compared using Unpaired t test (*p<0.05, **p<0.01, ***p<0.001). Density for Scrib1 t(38)=4.078, p<0.001 and ShScrib1: t(38)=3.334, p=0.0019; Intensity for Scrib1: t(38)=2.44, p=0.0196 and ShScrib1: t(38)=3.33, p=0.019.

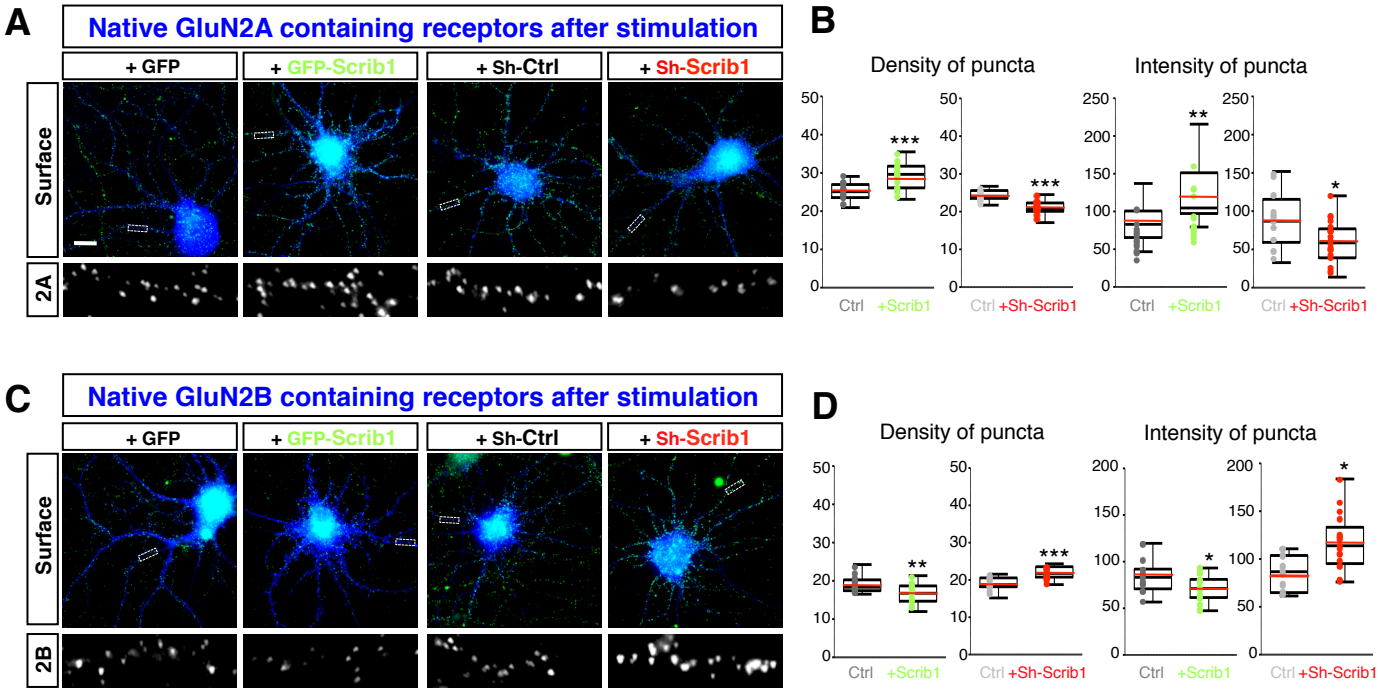

Figure S3. Scrib1 levels affect the surface expression of GluN2A- and GluN2B-containing receptors after stimulation. Related to Figure 3.

(**A,C**) The surface expression of GluN2A- (A) and GluN2B-containing NMDARs (C). Overexpression of GFP-control, GFP-Scrib1, Sh-Control or Sh-Scrib1 in primary hippocampal neuron cultures transfected with myc-GluN2A (A) or myc-GluN2B (C) at 14 to 15 DIV and stimulated with D-Serine/NMDA . Surface receptor populations are labelled in green (scale bar = 10µm).

(**B, D**) Box-and-whisker plots indicate the median value (black line) and mean value (red line), the 25-75th (box) and the 10-90th (whiskers); open circles represent individual values (n = 20 from at least 3 experiments). (B) Data were compared using Unpaired t test (*p<0.05, **p<0.01, ***p<0.001). Density for Scrib1: t(30)=4.27, p<0.001 and ShScrib1: t(33)=6.616, p<0.001; Intensity for Scrib1: t(30)=2.98, p=0.006 and ShScrib1: t(33)=2.62, p=0.013. (D) Data were compared using Unpaired t test (*p<0.05, **p<0.01, ***p<0.001). Density for Scrib1: t(32)=2.85, p=0.007 and ShScrib1: t(30)=4.847, p<0.001; Intensity for Scrib1: t(32)=259, p=0.014 and ShScrib1: t(30)=3.62, p=0.0011.

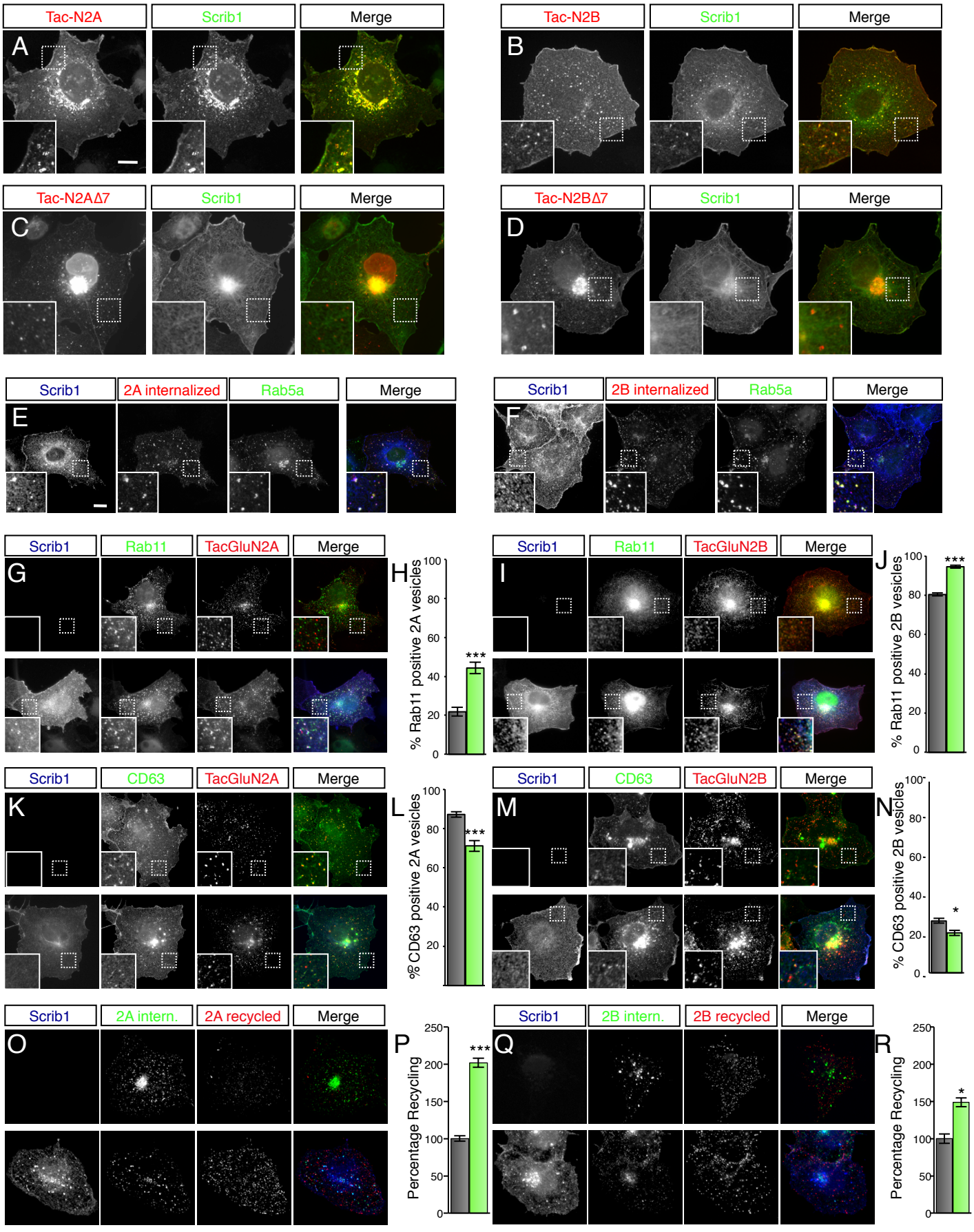
Tac-N2A
Scrib1
Merge
A
Tac-N2B
Scrib1
Merge
B
Tac-N2AΔ7
Scrib1
Merge
C
Tac-N2BΔ7
Scrib1
Merge
D
Scrib1
2A internalized
Rab5a
Merge
E
Scrib1
2B internalized
Rab5a
Merge
F
Scrib1
Rab11
TacGluN2A
Merge
G
H
% Rab11 positive 2A vesicles
100
80
60
40
20
0
***
Scrib1
Rab11
TacGluN2B
Merge
I
J
% Rab11 positive 2B vesicles
100
80
60
40
20
0
***
Scrib1
CD63
TacGluN2A
Merge
K
L
% CD63 positive 2A vesicles
100
80
60
40
20
***
Scrib1
CD63
TacGluN2B
Merge
M
N
% CD63 positive 2B vesicles
100
80
60
40
20
0
*
Scrib1
2A intern.
2A recycled
Merge
O
P
Percentage Recycling
250
200
150
100
50
0
***
Scrib1
2B intern.
2B recycled
Merge
Q
R
Percentage Recycling
250
200
150
100
50
0
*

Figure S4. Co-expression of Scrib1, Tac-GluN2A or Tac-GluN2B and endosomal markers in heterologous cells. Related to Figure 4 and Figure 5.

(**A-D**) Immunofluorescence microscopy of COS-7 cells transiently double-transfected with GFP-Scrib1 (green) and Tac-GluN2A, Tac-GluN2AΔ7, Tac-GluN2B or Tac-GluN2BΔ7 (red). GFP-Scrib1 and Tac-GluN2A colocalize at the plasma membrane and in cytoplasmic vesicle-like puncta (A), but GFP-Scrib1 does not colocalize with the truncated Tac-GluN2AΔ7 (C). GFP-Scrib1 and Tac-GluN2B colocalize at the plasma membrane and in cytoplasmic vesicle-like puncta (B), but GFP-Scrib1 does not colocalize with the truncated Tac-GluN2BΔ7 (D) (scale bar = 10µm).

(**E,F,G,I,K,M**) The labeling of Tac-GluN2A (E, G and K) or Tac-GluN2B (F, I and M) internalization (red) with the early endosome marker GFP-Rab5 (E and F, green), recycling endosome marker GFP-Rab11 (G and I, green) or late endosome marker GFP-CD63 (K and M, green) with or without HA-Scrib1 (blue). The cells with surface-labeled receptors were incubated at 37°C for 15 min for GFP-Rab5 staining and 30 min for GFP-Rab11 and GFP-CD63 staining.

(**H,J,L,N**) Quantification of (G), (I), (K) and (M). The histograms represent the means of the percentage of TacGluN2 vesicles that co-localize with the endosome markers GFP-Rab11 (H and J) or GFP-CD63 (L and M) ± sem. (H) Data were compared using Unpaired t test: n = 30 cells for each condition from 3 independent experiments; $t(58)=7.021$; $p<0.001$). (J) Data were compared using Unpaired t test: n = 30 cells for each condition from 3 independent experiments; $t(58)=14.22$; $p<0.001$). (L) Data were compared using Unpaired t test with Welch's correction: n = 20 to 25cells for each condition from 3 independent experiments; $t(43)=5.089$; $p<0.001$). (N) Data were compared using Unpaired t test: n = 10 cells for each condition from 3 independent experiments; $t(18)=3.299$; $p=0.0047$).

(**O,Q**) Labeling of recycled (red) and internalized (green) Tac-GluN2A (O) or Tac-GluN2B (Q) with or without Scrib1 (blue).

(**P, R**) Quantification of GluN2A (P) and GluN2B (R) recycling. The histograms represent the means of the percent recycling ± sem. Data were compared using Unpaired t test with Welch's correction: n = 20 to 35 cells for each condition from 3 independent experiments: $t(54)=4.985$; $p<0.001$ (p) and $t(67)=2.083$; $p<0.001$.

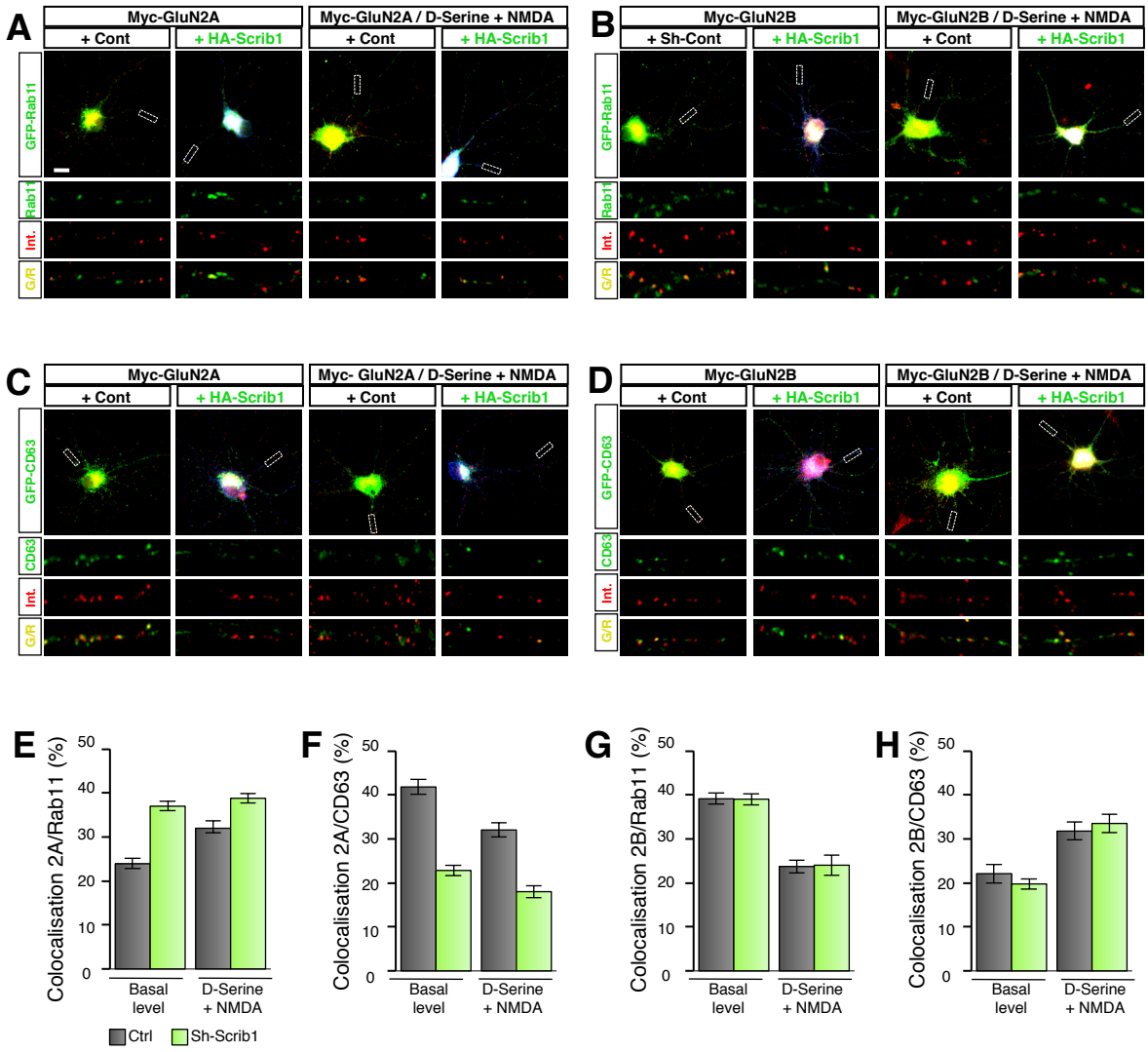

Figure S5. Overexpression of Scrib1 modifies GluN2A receptors endocytic sorting. Related to Figure 5.

(**A-D**) Internalization staining of transfected myc-GluN2A (A,C), and myc-GluN2B (B-D) with over-expression of recycling endosome marker GFP-Rab11 (A,B) or late endosomal marker GFP-CD63 (C,D) and Control or HA-Scrib1 in primary hippocampal neuron culture with or without stimulation (scale bar = 10µm).

(**E-H**) Histograms represent means of colocalization percentage of internalized receptor with endosome marker ± S.E.M.. After 30 min of internalization, the colocalization of GluN2A with GFP-Rab11 increases dependently of Scrib1 overexpression (Treatment effect: $F_{1,40}$=53.28, p<0.001) and stimulation (Stimulus effect: $F_{1,40}$=12.67, p<0.001) (E). The colocalization of GluN2A with GFP-CD63 decreases (Treatment effect: $F_{1,36}$=103.6, p<0.001, Stimulus effect: $F_{1,36}$=20.3, p<0.001) (F). No effect of Scrib1 overexpression on GluN2B colocalization with Rab11 was observed in normal or stimulated condition but the stimulation decreases the colocalization with of without Scrib1 (Stimulus effect: $F_{1,25}$ =79.54 for Rab11) (G). No effect of Scrib1 overexpression on GluN2B colocalization with CD63 was observed in normal or stimulated condition but the stimulation increases the colocalization with of without Scrib1 (Stimulus effect: $F_{1,23}$=38.77, p< 0.001 for CD63) (H). Data were compared using 2-way ANOVA (Stimulus effect and treatment effect, p<0.001, p<0.001, n = 10 to 15 from 3 experiments).

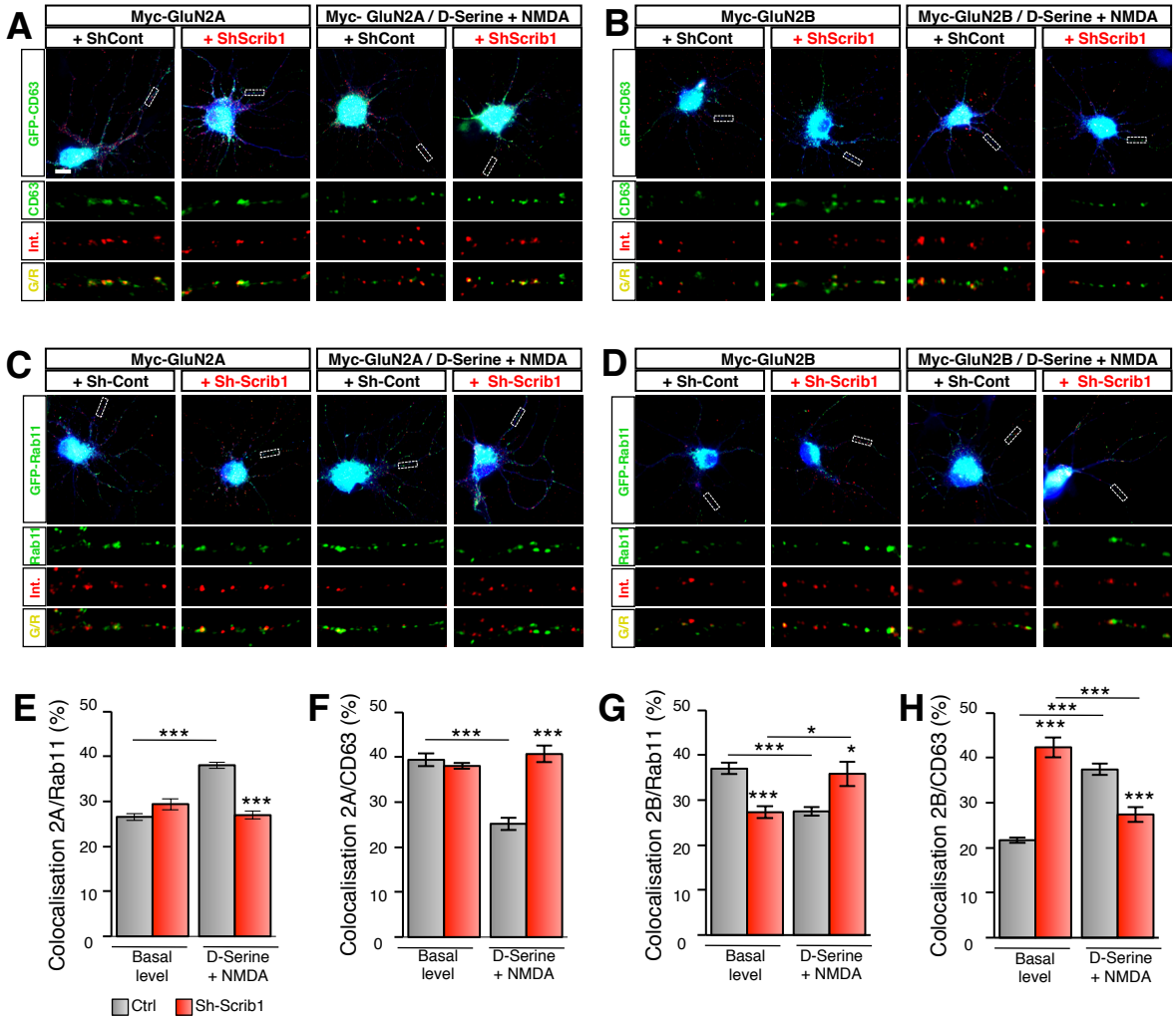

Figure S6. Down regulation of Scrib1 modifies differentially GluN2A and GluN2B-containing receptors endocytic sorting. Related to Figure 5.

(**A-D**) Internalization staining of transfected myc-GluN2A (A,C), and myc-GluN2B (B-D) with over-expression of the late endosomal marker CD63 tagged with GFP (A,B) or recycling endosome marker GFP-Rab11 (C,D) and Sh-Control or Sh-Scrib1 in primary hippocampal neuron culture and with or without stimulation scale bar = 10µm).

(**E-H**) Histograms represent means of colocalization percentage of internalized receptor with endosome marker ± S.E.M.. We showed that after 30 min of internalization the amount of colocalization of GluN2A with GFP-Rab11 or GFP-CD63 was the same with Sh-control or Sh-Scrib1 in basal condition and that stimulation decreased the traffic of GluN2A to Rab11 positive endosomes and increased the traffic of GluN2A to CD63 positive lysosomes (Interaction treatment x stimulus effect: $F_{1,34}$=53.43, Bonferroni corrected t test: ***p<0.001 for Rab11 and Interaction treatment x stimulus effect: $F_{1,35}$=36.27, Bonferroni corrected t test: ***p<0.001 for CD63 (E,F). In the presence of Sh-Scrib1, we observed that after 30 min of internalization the amount of colocalization of GluN2B and CD63 increased while the colocalization with Rab11 positive endosome decreased in basal condition (Interaction treatment x stimulus effect: $F_{1,31}$=21.9, Bonferroni corrected t test: ***p<0.001 for Rab11 and Interaction treatment x stimulus effect: $F_{1,32}$=112.19, Bonferroni corrected t test: ***p<0.001 for CD63) and that stimulation increased the traffic of GluN2B to Rab11 positive endosomes and decreased the traffic of GluN2B to CD63 positive lysosomes (Bonferroni corrected t test: *p<0.05 for Rab11; Bonferroni corrected t test: ***p<0.001 for CD63 (G,H). Data were compared using Two-way ANOVA (Stimulus effect and treatment effect), with Bonferroni post-hoc test *p<0,05 **p<0,005 ***p<0,001 (n = 10 to 15 from 3 experiments).

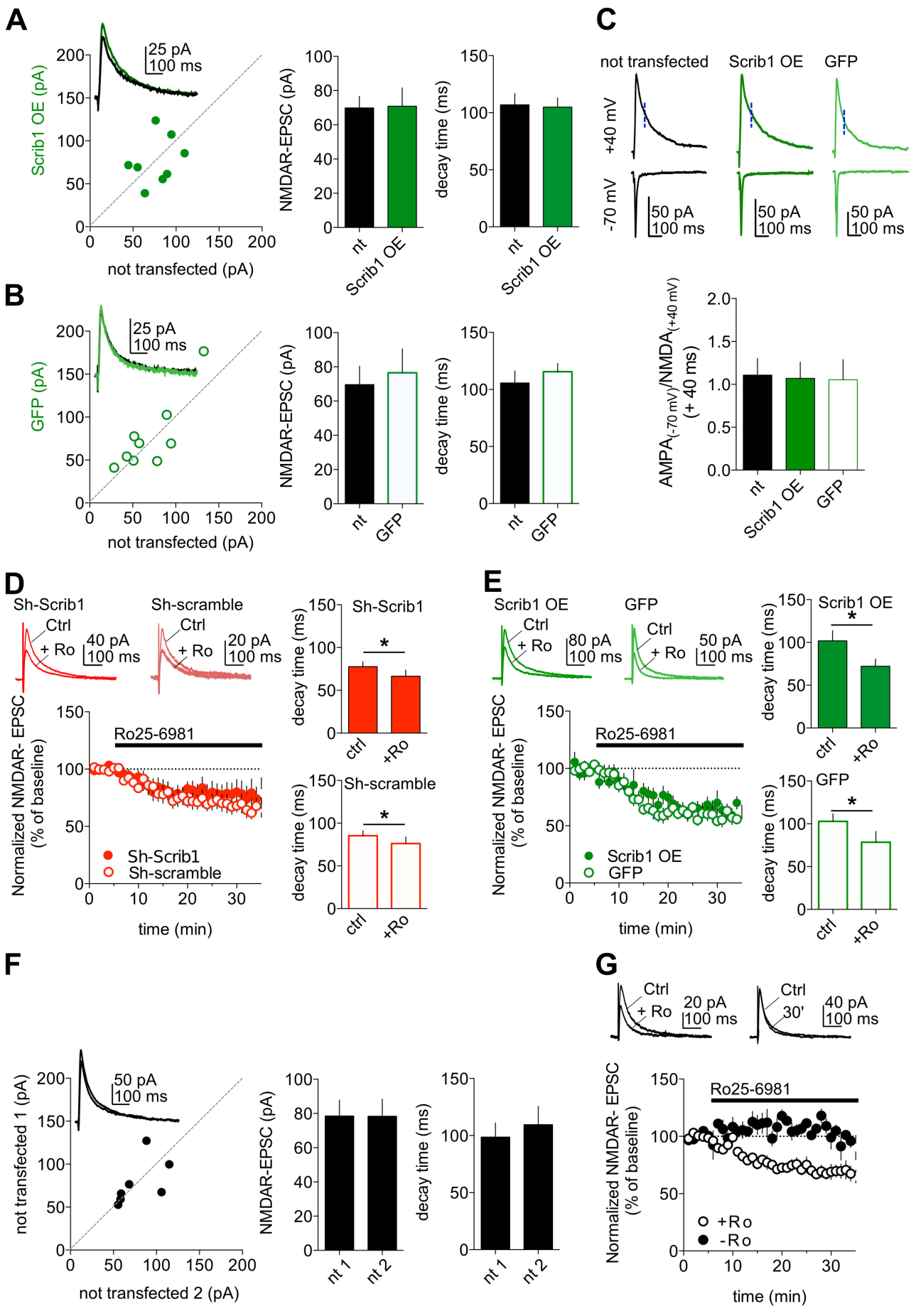
A
Scrib1 OE (pA)
not transfected (pA)
25 pA
100 ms
NMDAR-EPSC (pA)
decay time (ms)
nt
Scrib1 OE
B
GFP (pA)
GFP
C
not transfected
Scrib1 OE
GFP
+40 mV
-70 mV
50 pA
100 ms
AMPA(-70 mV)/NMDA(+40 mV) (+ 40 ms)
D
Sh-Scrib1
Sh-scramble
Ctrl
+ Ro
40 pA
20 pA
Ro25-6981
Normalized NMDAR- EPSC (% of baseline)
time (min)
ctrl
+Ro
E
Scrib1 OE
GFP
80 pA
50 pA
F
not transfected 1 (pA)
not transfected 2 (pA)
nt 1
nt 2
G
30'
20 pA
40 pA
+Ro
-Ro

Figure S7. Overexpression of Scrib1 does not regulate the level of NMDARs at Schaffer collaterals CA1 pyramidal cells synapse. Related to Figure 7.

(**A**) Transfection with Scrib1 does not affect neither the amplitude nor the decay time of NMDAR-mediates EPSCs at SC-CA1 synapse. Sample traces shown in the inset (control: 69.8±6.7 pA, n = 8; Scrib1: 70.8±10.8 pA, n = 8, Paired t test: NMDAR amplitude: t (8)=0.095, p=0.926; NMDAR decay: t (8)=0.606, p= 0.56).

(**B**) GFP transfection does not affect the NMDAR-mediates EPSCs at SC-CA1 synapse (amplitude and decay time), sample traces shown in the inset (control: 69.6±10.7 pA, n = 9; pSUPER -GFP: 76.5±13.9 pA, n = 9; Paired t test: NMDAR amplitude: t (8)=0.894, p=0.397; NMDAR decay: t (8)=0.919, p=0.384). (**C**) Sample traces and summary graphs illustrating that the AMPA/NMDA does not differ between not transfected cells and cells transfected with Scrib1 or pSUPER -GFP (not transfected: 1.11±0.19, n = 12; Scrib1: 1.81±0.38, n = 11; pSUPER –GFP: 1.05±0.23, n = 6).

(**D**) Sample traces and summary graph illustrating the effect of Ro25-2981 (1 μM) on NMDAR-mediated currents amplitude (pSUPER-ShRNA-Scrib1: 76.9±11.6 %, n = 9; pSUPER-ShRNA-control: 63.0±7.1 %, n = 8) and decay (pSUPER-ShRNA-Scrib1; baseline: 77.6±5.9 ms, after Ro25-2981: 66.5±7.3 ms, n = 9; pSUPER-ShRNA-control baseline: 85.3±5.8 ms, after Ro25-2981: 76.2±7.8 ms, n = 8; Paired t test: Ro effect on Sh-Scrib1 transfected cells: t (8)=2.963, p=0.018; Ro effect on pSUPER transfected cells: t (7)=2.373, p=0.049).

(**E**) Sample traces and summary graph illustrating the effect of Ro25-2981 (1 μM) on NMDAR-mediated currents amplitude (Scrib1: 76.9±11.6 %, n = 9; pSUPER-GFP: 63.0±7.1 %, n = 8) and decay (Scrib1: baseline: 77.6±5.9 ms, after Ro25-2981: 66.5±7.3 ms, n = 9; pSUPER-GFP baseline: 85.3±5.8 ms, after Ro25-2981: 76.2±7.8 ms, n = 8; Paired t test: Ro effect on Scrib1 transfected cells: t (8)=2.963, p=0.018; Ro effect on pSUPER -GFP transfected cells: t (7)=2.373, p=0.049).

(**F**) Sample traces and summary graphs illustrating that two randomly patched and adjacent not transfected neurons showed similar amplitude and decay time (n=7).

(**G**) Sample traces and summary graph illustrating the changes in amplitude of NMDAR-mediated currents amplitude in not transfected neurons in the presence (n=12) or absence (n=3) of Ro25-2981 (1 μM).

Proteins	Peptides	Kd (μM)	dG (kcal/mol)	dH (kcal/mol)	TdS Kcal/mol)
7PDZ1s	GluN2A WT	No interaction			
	GluN2B WT	No interaction			
7PDZ2s	GluN2A WT	60.0 ± 4.2	-5.7 ± 0.0	-7.1 ± 0.7	-1.4 ± 0.7
	GluN2A S1462A	No interaction			
	GluN2B WT	48.0 ± 7.8	-5.8 ± 0.1	-10.3 ± 0.9	-4.5 ± 1.1
	GluN2B S1480A	No interaction			
7PDZ3s	GluN2A WT	11.6 ± 2.3	-7.9 ± 1.7	-16.3 ± 1.1	-8.4 ± 0.6
	GluN2A S1462A	No interaction			
	GluN2B WT	12.3 ± 1.8	-7.2 ± 0.5	-14.7 ± 0.1	-8.8 ± 0.6
	GluN2B S1480A	No interaction			
7PDZ4s	GluN2A WT	202.5 ± 21.9	-5.4 ± 0.6	-5.4 ± 0.5	0.0
	GluN2A S1462A	No interaction			
	GluN2B WT	156.5 ± 16.3	-5.7 ± 0.4	-5.7 ± 0.4	0.0
	GluN2B S1480A	No interaction			
TRX (fusion protein)	GluN2A WT	No interaction			

Table S1. Thermodynamic Binding Parameters for Scrib1 PDZ domains and GluN2A or GluN2B peptides determined by ITC. Related to Figure 1.

Values are the arithmetic mean of at least two independent experiments (Kd: dissociation constant; G: Gibbs free energy ; H: enthalpy; S: entropy). All c-values were measured between 10 and 100. Stoichiometric (n) values ranged from 0.85 to 0.99.

Figure number	Conditions	Exact value (n)	Number of independent experiment	Error bars	Test	Degree of freedom & F/T Value	p value
2B	Ctrl,TTX,Biccuculin		3	SEM	Unpaired t-test		
	Scrib1	6				t(5)=4.547	p=0039
	GluN2A	6				t(5)=2.908	p=0.027
	GluN2B	6				t(5)=2.632	p=0.5507
2D	Ctrl vs. EOF		3	SEM	One sample t-test		
	Scrib1	5				t(4)=5.675	p=0.0024
	GAPDH	5				t(4)=0.92	p=0.39
2E	Ctrl vs. EOF		3	SEM	One sample t-test		
	GluN1	5				t(4)=0.3846	p=0.7163
	GluN2A	5				t(4)=0.2931	p=0.0326
	GluN2B	5				t(4)=0.0348	p=0.0348
2G	Ctrl vs. EOF		3	SEM	One sample t-test		
	GluN2A	4				t(3)=3.311	p=0.045
	GluN2B	6				t(5)=0.04756	p=0.96
3B	Ctrl	30	3	min-max	Kruskal-Wallis one way	F(2,85)=20.71	p<0.001
	Scrib1	28			Dunn's Multiple comparison:		
	Scrib1ΔPDZ2-3	30			Ctrl vs Scrib1		p<0.05
					Scrib1 vs Scrib1ΔPDZ2-3		p<0.001
3C	Ctrl	30	3	min-max	Kruskal-Wallis one way	F(2,85)=11.32	p<0.01
	Scrib1	28			Dunn's Multiple comparison:		
	Scrib1ΔPDZ2-3	30			Ctrl vs Scrib1		p<0.01
					Scrib1 vs Scrib1ΔPDZ2-3		p<0.05
3E	Ctrl	29	3	min-max	Kruskal-Wallis one way	F(2,84)=14.2	p<0.001
	Scrib1	28			Dunn's Multiple comparison:		
	Scrib1ΔPDZ2-3	30			Ctrl vs Scrib1		p<0.01
					Scrib1 vs Scrib1ΔPDZ2-3		p<0.01
3F	Ctrl	29	3	min-max	Kruskal-Wallis one way	F(2,84)=9.55	p<0.01
	Scrib1	28			Dunn's Multiple comparison:		
	Scrib1ΔPDZ2-3	30			Ctrl vs Scrib1		p<0.05
					Scrib1 vs Scrib1ΔPDZ2-3		p<0.05
3H	ShCtrl	29	3	min-max	Kruskal-Wallis one way	F(3,106)=60.42	p<0.001
	ShScrib1	30			Dunn's Multiple comparison:		
	Rescue	20			ShCtrl vs ShScrib1		p<0.001
	RescueΔPDZ2-3	30			ShScrib1 vs RescueΔPDZ2-3		p<0.001
					ShScrib1 vs Rescue		p<0.001
					Rescue vs RescueΔPDZ2-3		p<0.001
3I	ShCtrl	29	3	min-max	Kruskal-Wallis one way	F(3,106)=22.75	p<0.001
	ShScrib1	30			Dunn's Multiple comparison:		
	Rescue	20			ShCtrl vs ShScrib1		p<0.05
	RescueΔPDZ2-3	30			ShScrib1 vs RescueΔPDZ2-3		p<0.01
					ShScrib1 vs Rescue		p<0.01
					Rescue vs RescueΔPDZ2-3		p<0.01
3K	ShCtrl	30	3	min-max	Kruskal-Wallis one way	F(3,94)=31.31	p<0.001
	ShScrib1	26			Dunn's Multiple comparison:		
	Rescue	17			ShCtrl vs ShScrib1		p<0.01
	RescueΔPDZ2-3	22			ShScrib1 vs RescueΔPDZ2-3		p<0.01
					ShScrib1 vs Rescue		p<0.001
					Rescue vs RescueΔPDZ2-3		p<0.001
3L	ShCtrl	30	3	min-max	Kruskal-Wallis one way	F(3,94)=5.43	p=0.14
	ShScrib1	26			Dunn's Multiple comparison		
	Rescue	17					
	RescueΔPDZ2-3	22					
3N	Density:		3	min-max	Unpaired t-test:		
	Ctrl	24					
	Scrib1	26			Ctrl vs Scrib1	t(48)=0.598	p=0.55
	ShCtrl	15					
	ShScrib1	17			ShCtrl vs ShScrib1	t(30)=0.59	p=0.56
	Intensity:						
	Ctrl	24					
	Scrib1	26			Ctrl vs Scrib1	t(48)=0.197	p=0.84
	ShCtrl	15					
	ShScrib1	17			ShCtrl vs ShScrib1	t(30)=0.051	p=0.96
3P	Density:		3	min-max	Unpaired t-test:		
	Ctrl	15					
	Scrib1	15			Ctrl vs Scrib1	t(28)=0.61	p=0.54
	ShCtrl	15					
	ShScrib1	15			ShCtrl vs ShScrib1	t(28)=1.25	p=0.22
	Intensity:						
	Ctrl	15					
	Scrib1	15			Ctrl vs Scrib1	t(28)=0.19	p=0.85
	ShCtrl	15					
	ShScrib1	15			ShCtrl vs ShScrib1	t(28)=1.94	p=0.063
4F	Ctrl	20	3	SEM	Two-way Anova:		
	Scrib1	19			Treatment	F(1,74)=3.839	p=0.54
	Ctrl-Stim	20			Stimulus	F(1,74)=75.625	p<0.001
	Scrib1-Stim	19			Interaction treatment x stimulus effect	F(1,74)=0.125	p=0.724
4G	ShCtrl	15	3	SEM	Two-way Anova:		
	ShScrib1	18			Interaction treatment x stimulus effect	F(1,68)=5.072	p=0.027

	ShCtrl-Stim ShScrib1-Stim	20 19			Bonferroni's Multiple Comparison Test: ShCtrl vs ShScrib1 ShCtrl vs ShCtrl-Stim ShCtrl vs ShScrib1-Stim		 p<0.001 p<0.001 p<0.001
4H	Ctrl Scrib1 Ctrl-Stim Scrib1-Stim	20 16 20 16	3	SEM	Two-way Anova Treatment Stimulus Interaction treatment x stimulus effect	 F(1,69)=0.101 F(1,69)=0.375 F(1,69)=0.781	 p=0.75 p=0.54 p=0.38
4I	ShCtrl ShScrib1 ShCtrl-Stim ShScrib1-Stim	17 16 16 15	3	SEM	Two-way Anova: Interaction treatment x stimulus effect Bonferroni's Multiple Comparison Test: ShCtrl vs ShScrib1 ShScrib1 vs ShScrib1-Stim	 F(1,60)=15.252	 p<0.001 p<0.001 p=0.0011
4K	ShCtrl Rescue	15 17	3	SEM	Unpaired t-test	t(30)=0.451	p=0.66
4M	ShCtrl Rescue	17 17	3	SEM	Unpaired t-test	t(32)=2.524	p=0.017
5F	Ctrl Scrib1 Ctrl-Stim Scrib1-Stim	18 17 18 17	3	SEM	Two-way Anova Treatment Stimulus Interaction treatment x stimulus effect	 F(1,66)=44.318 F(1,66)=9.564 F(1,66)=0.0036	 p<0.001 p=0.0029 p=0.95
5G	ShCtrl ShScrib1 ShCtrl-Stim ShScrib1-Stim	13 15 15 13	3	SEM	Two-way Anova: Interaction treatment x stimulus effect Bonferroni's Multiple Comparison Test: ShCtrl vs ShCtrl-Stim ShCtrl vs ShScrib1-Stim	 F(1,51)=6.993	 p=0.011 p=0.016 p=0.0138
5H	Ctrl Scrib1 Ctrl-Stim Scrib1-Stim	18 15 15 15	3	SEM	Two-way Anova Treatment Stimulus Interaction treatment x stimulus effect	 F(1,59)=0.069 F(1,59)=29.632 F(1,59)=0.017	 p=0.79 p<0.001 p=0.90
5I	ShCtrl ShScrib1 ShCtrl-Stim ShScrib1-Stim	20 17 15 18	3	SEM	Two-way Anova: Interaction treatment x stimulus effect Bonferroni's Multiple Comparison Test: ShCtrl vs ShScrib1 ShCtrl vs ShCtrl-Stim ShCtrl vs ShScrib1-Stim	 F(1,66)=47.216	 p<0.001 p<0.001 p=0.0148 p<0.001
5K	Ctrl-ARF6 Scrib1-ARF6 Ctrl-ARF6DN Scrib1-ARF6DN	20 19 20 15	3	SEM	Two-way Anova: Interaction treatment1 x treatment2 Bonferroni's Multiple Comparison Test: Ctrl-ARF6 vs Scrib1-ARF6 Ctrl-ARF6 vs Ctrl-ARF6DN Ctrl-ARF6 vs Scrib1-ARF6DN	 F(1,69)=4.98	 p=0.0289 p=0.0134 p<0.001 p<0.001
5M	Ctrl-EFA6 Scrib1-EFA6 Ctrl-EFA6DN Scrib1-EFA6DN	10 10 10 10	3	SEM	Two-way Anova Interaction treatment1 x treatment2 Bonferroni's Multiple Comparison Test: Ctrl-EFA6 vs Scrib1-EFA6 Ctrl-EFA6 vs Ctrl-EFA6DN Ctrl-EFA6 vs Scrib1-EFA6DN	 F(1,36)=8.85	 p=0.0052 p<0.001 p<0.001 p<0.001
6J	Ctrl Scrib1 Scrib1Y834A	20 19 20	3	SEM	One-way Anova Bonferroni's Multiple Comparison Test: Ctrl vs Scrib1 Ctrl vs Scrib1Y834A	F(2,56)=18.846	p<0.001 p<0.001 p<0.001
6K	Ctrl Scrib1 Scrib1Y834A	15 18 15	3	SEM	One-way Anova Bonferroni's Multiple Comparison Test: Ctrl vs Scrib1 Ctrl vs Scrib1Y834A	F(2,45)=29.623	p<0.001 p<0.001 p<0.001
7B	Ctrl ShScrib1	9 9	6	SEM	Paired t-test NMDA amplitude: NMDA decay:	t(8)=2.964 t(8)=0.771	p=0.018 p=0.46
7C	Ctrl ShCtrl	9 9	6	SEM	Paired t-test NMDA amplitude: NMDA decay:	 t(8)=0.423 t(8)=1.391	 p=0.68 p=0.2
7D	ShScrib1 ShCtrl	11 10	7	SEM	Unpaired t-test (Mann Whitney)	U=26	p=0.043
7E	Ctrl ShScrib1	6 6	4	SEM	Paired t-test	t(8)=1.323	p=0.24
7F	Ctrl ShCtrl	6 6	4	SEM	Paired t-test	t(8)=0.376	p=0.72

Table S2. Statistics reporting, by figure

SUPPLEMENTAL EXPERIMENTAL PROCEDURES

Antibodies

The following primary antibodies were used in this study: anti-Scrib1 antibody (AbMM468) (Montcouquiol et al., 2006); anti-Scrib1 (C20, sc-11049, Santa Cruz Biotechnology); anti-GluN1 (clone 54.1, 556308, BD Pharmingen, San Diego, CA); anti-GluN2A C-ter (clone 5530, gift from G. Köhr); anti-GluN2B (610417, BD Biosciences); anti-GluN2A N-ter and GluN2B N-ter (Groc et al., 2006); anti-GluN2B (AGC-003, Alomone Labs); anti-GABA(A) α1 extracellular (AGA-001, Alomone Labs); anti-Densin-180 (G1, sc-390153, Santa Cruz Biotechnology), anti-Erbin and anti-Lano (gift from J.P. Borg); anti-$GABA_A$ receptor β3 subunit (75-149, NeuroMab, gift from M. Garret); anti-AP50 (611350, BD Transduction lab); anti-Tac (Sans et al., 2005); anti-myc mouse 9E11 (MMS-164P, Covance); anti-GFP (AB3080P, Merck-Millipore). Secondary antibodies used as follows: Alexa Fluor 488, 546 and 470 conjugated antibodies (Invitrogen), AMCA, FITC, Cy3 conjugated antibodies (Jackson Immunoresearch Laboratories); biotin conjugated antibodies (Vector Laboratories); HRP conjugated antibodies (GE Healthcare).

Vector constructions

Full-length human Scribble, cloned in pEGFP-C1, was generously provided by Prof. Ian Macara (UVA, Charlottesville, VA, USA). Mutated forms of GFP-Scribble1 were generated using the Quick Change site-directed mutagenesis kit (Stratagene). Scrib1-ΔPDZ2-3 is a truncated form of hScrib1 lacking both PDZ domains #2 and #3 (amino acids 1-301) that was generated by site-directed mutagenesis using the GFP-Scrib1 as template and the following primer:
5'cccgggcccctccgtcagcgccacgcacccccgggcctacgggaa3'. Cloning and mutagenesis were verified by sequencing for all constructions. The Super-GFP plasmids were purchased from Oligoengine. Tac-GluN2A, Tac-GluN2AΔ7, Tac-GluN2B, Tac-GluN2BΔ7, Myc-GluN2A and myc-GluN2B were used previously (Lavezzari et al., 2004; Prybylowski et al., 2005; Roche et al., 2001; Sans et al., 2005). GFP-Rab5 and GFP-Rab11 were generously provided by Dr Philip D. Stahl (Washington University School of Medicine, St Louis, Missouri, USA), GFP-CD63 by Dr Thierry Galli (INSERM ERL U950, Paris, France), and myc-$GABA_A$ β3 by Dr Maurice Garret (INCIA, Bordeaux, France); $ARF6^{WT}$-HA and $ARF6^{T27N}$-HA were from Addgene and EFA6 wt and E242K were from Dr Frédéric Luton (IPMC, CNRS, Nice, France).

Protein production and purification for isothermal titration calorimetry (ITC)

The gene encoding full-length, wild-type mouse Scrib1 was used as a template to generate PCR products corresponding to each of the four individual PDZ domains of Scrib1 (PDZ1-PDZ4). These products were cloned into a pET28a+ vector modified to be used as a ligation-independent cloning (LIC) system, confirmed by DNA sequencing and expressed in *E. coli* BL21 cells to produce the PDZs as thioredoxin fusion proteins. Creating the PDZ-thioredoxin fusion proteins allowed quantification by UV spectrophotometry, which would have been impossible for some isolated PDZs because some of them have no aromatic residues. The expressed proteins were purified using immobilized Ni^{2+} affinity chromatography followed by SEC on Superdex S200 (or S75) columns (GE Healthcare) in ITC buffer containing 250 mM NaCl, 20 mM Hepes pH 7.5 and 2 mM DTT at 4°C, then concentrated. Purified proteins were confirmed by SDS-PAGE and MALDI mass spectrometry. The 12-residue C-terminal peptides of the NMDAR subunits (GluN2A, $GluN2A^{S1462A}$, GluN2B or $GluN2B^{S1480A}$) were purchased from GeneCust. ITC experiments were performed on an ITC_{200} (GE Healthcare). For each run, 43 injections of 1 µl of 1.5 to 3 mM peptide solutions were added at 100-second intervals from a stirring syringe into the sample cell containing 200 µl of 120 to 250 µM PDZ domains. The peptides were dissolved in ITC buffer and readjusted to pH 7.5 when necessary. Both protein and peptide solutions were extensively degassed. The experiments were performed with a reference power of 10 µcal/s and a sample cell temperature of 20°C. The titration curves were analyzed using the ORIGIN 7.0 software

(MicroCal Inc.). The experimental data were corrected for the effects of peptide dilution by subtracting the curve obtained by the titration of the peptide solution into buffer alone. All protein concentrations were determined by absorbance measurements at 280 nm using calculated molar extinction coefficients. ITC was used as it allows a fine determination of the dissociation constants between a protein and a target peptide. However this is obtained at the expense of significant sample volume and concentration. As we were only concerned by: a) finding out which PDZ could bind the target peptides and b) a ranking of very different affinities between different PDZs, two experiments were thus enough for our purpose: n = 2 allowed to rule out any large experimental mistake and confirm the ranking order of the Kds. Supplementary determinations using ITC would have required significant amount of material to perform several extra determinations and only result in a marginally increased accuracy of no consequence on our interpretation.

Pull-down assays

Scrib1$^{PDZ1\text{-}PDZ4}$ containing the AP2μ interacting motif, the mutated form Scrib1$^{PDZ1\text{-}PDZ4\text{-}Y834A}$ and full length AP2μ were cloned in a modified pET28 plasmid then expressed in E.Coli BL21 DE3 RIPL at 17°C in ZYP media overnight. Proteins were purified on His Trap HP columns (GE Healthcare), followed directly by gel filtration on Superdex 75 (GE Healthcare). The Scrib1$^{PDZ1\text{-}PDZ4}$ and Scrib1$^{PDZ1\text{-}PDZ4\text{-}Y834A}$ constructs were desalted treated with TEV protease then passed over a His Trap HP column to fix the uncut material, TEV protease and cleaved His tag. The flow through of this second pass on His Trap HP, which contains cleaved Scrib1 constructs, was further purified on a Superdex75 column (GE Healthcare). All purified proteins were >95% pure as assessed by SDS PAGE and identities were confirmed using MALDI. Talon magnetic beads with 50 µg of His-tagged AP2μ protein were incubated with Scrib1 or Scrib1^{Y834A} in 50 mM Tris pH 8, 250 mM NaCl, 25 mM imidazole and incubated for 60 min at 4°C. Beads were then washed extensively with 50 mM Tris pH 8, 250 mM NaCl, 25 mM imidazole. Bound protein complexes were eluted from the beads with 5 µl of buffer containing 500mM of imidazole, and then mixed with SDS-PAGE sample buffer before SDS-PAGE and Coomassie coloration.

Bioinformatics analysis and modeling

To build a model of residues 830 to 839 of Scrib1 and AP2µ, a starting model was constructed using the structure of AP2µ complexed with residues 197 to 206 from the CTLA-4 internalization peptide (PDB 1H6E) (Follows et al., 2001). There are several structures of PDB showing AP2µ complexed with peptides from different partners, and all of them have a conserved Tyr residue bound to a hydrophobic pocket in AP2µ. This Tyr is also present in the Scrib1 region responsible for the interaction with AP2µ, so this Tyr position was kept and used as a reference point to build our model. We first mutated the sequences from CTLA-4 to those of Scrib1. An initial analysis of the structure confirmed that, in addition to Tyr binding, we could model several ionic bonds between AP2µ and Scrib1. Using this new PDB file as a starting model, we first ran the geometry regularization module from the PhoeniX suite (Adams et al., 2010) to remove obvious steric clashes. Then, we used coot (Emsley et al., 2010) to build a model that would take into account the existence of ionic bonds and checked the quality of the model using MolProbity (DeLano et al., 2002). The final model did not show clashes between µ2-AP2 and the Scrib1 peptide. We used PyMOL to prepare the figures (Stoppini et al., 1991).

Detergent solubilization and immunoprecipitation experiment

IP experiments were performed after 1% sodium deoxycholate (DOC), 0.1% Triton X-100 solubilization as described previously (Wenthold et al., 1996; Sans et al., 2003). Briefly, hippocampi from rat were homogenized with a polytron in 50 mM Tris-HCl, pH 7.4, containing a protease inhibitor mixture (Roche). Membranes were sedimented by centrifugation (100,000 x g; 30 min; 4°C), solubilized in 1% DOC, 50 mM Tris-HCl, 1 mM EDTA, pH 8.1, for 30–45 min at 37°C, and before

insoluble material was removed by centrifugation, 0.1% Triton X-100 was added. For immunoprecipitation, 40 µl of polyclonal anti-goat Scrib1 antibodies (C20) were attached to protein-A/G beads. Protein-A/G beads were then pelleted, washed in PBS plus 0.1% Triton X-100, and incubated with 1.4 ml of the DOC-solubilized tissue at 4°C with constant rotation. The beads were then washed three times with 50 mM Tris-HCl, pH 7.5, containing 0.1% Triton X-100 and 150 mM NaCl and, then, were boiled in 100 µl of 2X SDS-PAGE sample buffer for 5 min as described by Sans et al. (2003). Experiments were repeated more than 3 times. Samples were analyzed by SDS/PAGE and immunoblotting.

Subcellular fractionation from cortical neurons

Synaptosomes from cultured cortical neurons were prepared using a small-scale modification of this procedure. For subcellular fractionation, hippocampi were homogenized in Buffer A (0.32 M sucrose, 0.05 M Tris-HCl, pH 7.5, 10 mM EDTA, containing a protease inhibitor mixture). The homogenate was subfractionated by centrifugation at 1,000 x g for 15 min and the supernatant S1 removed and further centrifuged at 10,000 x g for 20 min to obtain P2. The P2 pellet was resuspended in hypotonic buffer B (0.05 M Tris-HCl, pH 7.5, containing a protease inhibitor mixture) and incubated for 30 min on ice, briefly sonicated, and 2 M sucrose was added to make a final concentration of 1.3 M. The lysate was overlaid with a layers of 0.8 M sucrose and 0.32 M sucrose and centrifuged at 60,000 x g for 20 min. Synaptic membranes were recovered from the 1.3 M and 0.8 M sucrose interface.

Synaptosome extraction after new environment stimulation

Experiments were done using 10 week-old male Sprague Dawley rats (n = 12). All subjects were housed in groups of 2 per cage for 2 weeks before starting the experiments, in standard laboratory conditions with a 12 h light/12 h dark cycle (light on: 07:00) with food and water supplied ad libitum. Rats were exposed to the enriched open field (EOF) for 10 min. During the same period, control rats were left in their home cage. At the end of the test, all rats returned in their home cage and left undisturbed for 60 min. Then, rats were anesthetized by brief inhalation of isoflurane (0.05% in air) and sacrificed by decapitation. The hippocampus was rapidly dissected and homogenized in 50 mM Tris HCl, pH 7.4, containing a cocktail of protease inhibitors (Roche). P2 subcellular fractionation was performed as described previously (Sans et al., 2003).

Culture and Transfections of HEK-293 or COS-7 cells

HEK-293 (ATCC® CRL-1573™) or COS-7 (ATCC® CRL1651™) cells were cultured in DMEM (Invitrogen) supplemented with FCS and antibiotics. Transfections were done using the calcium phosphate coprecipitation method (Sans et al., 2003).

Surface, internalization, and recycling experiments in fibroblasts

For surface labeling, the cells were incubated live with Tac monoclonal antibodies for 1 h at 4°C, washed with PBS and blocked with 10% NGS before applying the secondary antibody. The cells were then fixed with 4% paraformaldehyde in PBS, permeabilized in PBS containing 0.25% Triton X-100 for 5 min, and blocked in 10% normal goat serum (NGS) in PBS/0.1% Triton X-100 for 1 h. The cells were incubated with a primary antibody in PBS containing 3% NGS for 1 h, washed and incubated with secondary antibodies for 30 min in 3% NGS/PBS. The GFP immunofluorescence was visualized with an FITC filter.

To measure internalization, after labeling the surface receptors for 1 h at 4°C and the PBS washes, the cells were returned to 37°C for internalization. After 5 to 30 min, the cells were chilled with ice-cold PBS and exposed to 0.5 M NaCl/0.2 M acetic acid for 4 min at 4°C to remove the remaining labeling from the surface. The cells were incubated with excess unconjugated secondary antibody to block all remaining surface receptors. After a PBS wash, the cells were fixed in 4% paraformaldehyde in PBS,

washed with PBS and permeabilized in 0.25% Triton X-100 for 5 min. The coverslips were then incubated with FITC- or Cy3-conjugated anti-mouse secondary antibodies for 30 min.
For the recycling assays, after stripping, the cells were incubated at 37°C for 30 min in the presence of a fluorophore-conjugated secondary antibody to visualize the internalized receptors that had recycled back to the plasma membrane. The cells were then fixed, permeabilized and incubated with a second fluorescent secondary antibody to visualize the internalized receptors that had failed to recycle back to the plasma membrane. The average fluorescence of the recycled receptors and internalized receptors was then determined and plotted as a ratio (recycling index).

Surface, internalization, and recycling experiments in neurons
For surface labelling, an anti-myc antibody (Covance) was applied to live cells for 1 h at room temperature. Neurons were then washed with Neurobasal before applying the secondary antibody and then fixed and processed for total staining**.**
For the internalization and recycling experiments, The hippocampal neurons were incubated with mouse anti-myc antibody (1: 1000, Invitrogen) at RT for 20 min and then incubated at 37°C for 30 min to allow internalization of receptors (after stimulation or not). For internalisation staining, neurons were fixed and incubated for 30 min with Alexa Fluor 647-conjugated anti-mouse secondary antibody before blocking with excess of unconjugated anti-mouse IgG Fab for 20 min. For recycling staining, non-internalized surface bound antibody was then blocked with excess of unconjugated anti-mouse IgG Fab at RT for 20 min. Neuron were then incubated at 37 °C for 1 h to allow recycling back to the plasma membrane. Neurons were fixed and incubated for 30 min with Alexa Fluor 647-conjugated anti-mouse secondary antibody to label the recycled surface population of receptors before permeabilization. Remaining surface primary antibodies were blocked with excess of unconjugated anti-mouse IgG Fab (1:50). After permeabilization, neurons were incubated with Alexa Fluor 546-conjugated anti-mouse secondary antibody to label the internalized population of receptors.

Fluorescence Microscopy
Images were acquired with a Leica DM6000 microscope equipped with a CoolSNAPHQ2 camera (PhotoMetrics) and MetaMorph 7.5 software (Universal Imaging) or with a Zeiss AxioImager Z1 equipped with an AxioCam MRm and the Zeiss software. All quantitation was done using MetaMorph 7.5 software on isolated dendrites. The number of puncta or intensity was calculated from 5 different regions of a 20-µm length per neuron and averaged. Statistical significance was determined using a Student's unpaired t-test or ANOVA one-way with Bonferroni post-hoc test.

Pre-embedding immunocytochemistry
Three Sprague Dawley male rats (~3 week old) of approximately 150 g were used. After terminal anesthesia was induced by brief inhalation of isoflurane (0.05% in air), followed by an intramuscular injection of ketamine (100 mg kg^{-1}) and xylazine (10 mg kg^{-1}), rats were intracardially perfused with 4% paraformaldehyde and 0.1% glutaraldehyde in PBS (0.1 M, pH 7.2), and brain sections (100 µm) were cut on a Leica VT1000S vibratome (Leica Microsystems, Milton Keynes, UK). All procedures were performed according to the requirements of the United Kingdom Animals (Scientific Procedures) Act 1986, the European Communities Council Directives (86/609/EEC) and the French national Committee (87/848) recommendations. The immunolabeling method has been described previously (Moreau et al., 2010). Briefly, the sections were immunolabeled with Scrib1 polyclonal antibody (AbMM468) (Montcouquiol et al., 2006), followed by a biotinylated secondary antibody, ABC Elite Kit (Vector Laboratories), and the peroxidase reaction was revealed by VIP substrate Kit (Vector Laboratories). Then the sections were osmicated, dehydrated, and flat embedded in Durcupan resin (Sigma-Aldrich). Ultrathin sections (70–90 nm) were countercolored with uranyl acetate and lead citrate. Experiments were repeated three times per animal. Control experiments, in which the primary antibody was omitted, resulted in no immunoreactivity.

Post-embedding immunogold

Three Sprague Dawley male rats (3 week old) were terminally anesthetized and intracardially perfused with 4% paraformaldehyde and 0.5% glutaraldehyde in PBS (see above). The post-embedding immunogold method has been previously described (Sans et al., 2003; Sans et al., 2001; Sans et al., 2005). Briefly, after perfusion, the brains were sectioned, and cryoprotected. Sections were then frozen in a Leica CPC cryofixation system and freeze-substituted into Lowicryl HM-20 (EMS) in a Leica automatic freeze-substitution system (AFS). For double-labeling, sections were incubated with Scrib1 polyclonal antibody (AbMM468) (Montcouquiol et al., 2006) and GluN1 monoclonal antibody (556308, BD Pharmingen), followed by 5-nm goat anti-rabbit and 15-nm goat anti-mouse immunogold (British Biocell Intl.). Experiments were repeated three times per animal. Control experiments, in which the primary antibodies were omitted, resulted in no immunoreactivity.

Slice culture preparation and transfection for electrophysiological recordings

Organotypic hippocampal slice cultures were prepared from P5-P7 Sprague Dawley rats. Three to four days after plating, the medium was replaced and then changed every 2-3 days. After 7-9 days in vitro we performed single cell electroporation (SCE) to transfect individual cells with cDNAs encoding pSuperGFP (to localize transfected neuron) and pSUPER-ShRNA-Scrib1 or pSUPER-ShRNA-control or Scrib1. Plasmids (100 ng/µl) were dissolved in a filtered K^+-based intracellular solution to fill 6-9 MΩ patch clamp pipettes. Electroporation was performed in a pre-warmed HEPES based ACSF by the delivery of 50-100 square-pulses (600 µs duration) at 100 Hz with an amplitude of -10 mV. Electrophysiological recording were performed 3 days after transfection.

Electrophysiological recordings in slice and data analysis

Whole-cell voltage–clamp recordings (3.5 to 4.5 MΩ electrodes) were made at 30-32°C from CA1 pyramidal cells visualized by infrared videomicroscopy. Transfected cells were recognized by the GFP fluorescence. Slices were perfused with an extracellular solution composed of 125 mM NaCl, 2.5 mM KCl, 1.25 mM NaH_2PO_4, 26 mM $NaHCO_3$, 2.3 mM $CaCl_2$, 1.3 mM $MgCl_2$, and 25 mM glucose saturated with 95% O_2/5% CO_2. NMDAR-mediated currents were recorded in the presence of NBQX (20 µM), bicuculline (10 µM) and N6-cyclopentyladenosine (50-100 nM) to reduce polysynaptic activity. The intracellular solution was composed of: 140 mM cesium methanesulfonate, 2 mM $MgCl_2$, 4 mM NaCl, 5 mM phospho-creatine, 2 mM Na_2ATP, 0.2 mM EGTA, 10 mM HEPES, 0.33 mM GTP (pH 7.3). Schaffer collateral-CA1 synapses were stimulated with a glass pipette positioned 100-150 µm from the recorded neurons. Small, hyperpolarizing voltage/current steps were given before each afferent stimulus allowing online monitoring of input and series resistance. The access resistance was <20 MΩ, and cells were discarded if it changed by >20%. NMDAR-mediated EPSCs decay time was calculated with a single weighted decay measure (referred in the text as decay time) and calculated from the area under the peak-normalized current for 0.7 s after the peak. For AMPA/NMDA ratio, NMDAR-mediated EPSCs were measured 50 ms after the initiation of the EPSC, a time point at which AMPAR-mediated currents are absent or minimal. No series resistance compensation was used. Recordings were made using EPC 9 and 10 amplifiers (HEKA Elektronik, Lambrecht/Pfalz, Germany) and were filtered at 0.5–1 kHz, digitized at 5 kHz, and stored on a personal computer. Analysis was performed using Neuromatic (www.neuromatic.thinkrandom. com) written within the Igor Pro 6.0 environment (WaveMetrics, Lake Oswego, OR). Values are presented as mean ± s.e.m.. Either a paired or unpaired Student's t-test was used to define statistical differences between values.

Data presentation and statistical analysis

For each representative image (including western-blot and immunostaining), experiment results were successfully repeated with at least 3 independent experiments, except if stated otherwise. Sample size was determined using the Mead's resource equation method or using a formal method such as

power analysis. For data analysis, quantifications were performed using randomly selected transfected COS-7 and HEK-293 cells or neurons. Data are presented in the text as mean ± s.e.m. or whiskers boxes. When it was appropriate, plotting independent data points was considered as more informative. Details of statistical analyses and n values are provided in the methods subsections referring to method used. Statistical analyses were performed using the Statistica or GraphPad Prism statistical package (GraphPad, San Diego, CA). Normality of distribution and homogeneity of variance were validated and unpaired Student's two-tailed t-test for two data sets were used to compare groups with similar variance and are indicated along the p values in figures. $p<0.05$ was considered statistically significant. Statistics were derived from at least 3 independent experiments. See Table S2.

Supplemental References

Adams, P.D., Afonine, P.V., Bunkóczi, G., Chen, V.B., Davis, I.W., Echols, N., Headd, J.J., Hung, L.-W., Kapral, G.J., Grosse-Kunstleve, R.W., McCoy A.J., Moriarty, N.W., Oeffner, R., Read, R.J., Richardson, D.C., Richardson, J.S., Terwilliger, T.C. and Zwart P.H. (2010). PHENIX: a comprehensive Python-based system for macromolecular structure solution. Acta Cryst. D66, 213-221.

DeLano, W.L. (2002) The PyMOL Molecular Graphics System. http://www.pymol.org/

Montcouquiol, M., Sans, N., Huss, D., Kach, J., Dickman, J.D., Forge, A., Rachel, R.A., Copeland, N.G., Jenkins, N.A., Bogani, D., et al. (2006). Asymmetric localization of Vangl2 and Fz3 indicate novel mechanisms for planar cell polarity in mammals. J Neurosci 26, 5265-5275.

Sans, N., Racca, C., Petralia, R.S., Wang, Y.X., McCallum, J., and Wenthold, R.J. (2001). Synapse-associated protein 97 selectively associates with a subset of AMPA receptors early in their biosynthetic pathway. J Neurosci 21, 7506-7516.

Stoppini, L., Buchs, P.A., and Muller, D. (1991). A simple method for organotypic cultures of nervous tissue. J Neurosci Methods 37, 173-182.